Proteomics-based determination of double stranded RNA interactome reveals known and new factors involved in Sindbis virus infection

Erika Girardi[1, *], Mélanie Messmer[1], Paula Lopez[1], Aurélie Fender[1], Johana Chicher[2], Béatrice Chane-Woon-Ming[1], Philippe Hammann[2], Sébastien Pfeffer[1, *]

[1] Université de Strasbourg, Architecture et Réactivité de l'ARN, Institut de Biologie Moléculaire et Cellulaire du CNRS, 2 allée Konrad Roentgen, 67084 Strasbourg France

[2] Université de Strasbourg, Institut de Biologie Moléculaire et Cellulaire du CNRS, Plateforme Protéomique Strasbourg – Esplanade, 2 allée Konrad Roentgen, 67084 Strasbourg France

* To whom correspondence should be addressed: e.girardi@ibmc-cnrs.unistra.fr; s.pfeffer@ibmc-cnrs.unistra.fr

Keywords: dsRNA, proteomics, Sindbis virus, dsRNAome, SFPQ, RNA binding protein

Running title: dsRNA interactome of Sindbis virus infected cells

Abstract

Viruses are obligate intracellular parasites, which depend on the host cellular machineries to replicate their genome and complete their infectious cycle. Long double stranded (ds)RNA is a common viral by-product originating during RNA virus replication and is universally sensed as a danger signal to trigger the antiviral response. As a result, viruses hide dsRNA intermediates into viral replication factories and have evolved strategies to hijack cellular proteins for their benefit. The characterization of the host factors associated with viral dsRNA and involved in viral replication remains a major challenge to develop new antiviral drugs against RNA viruses. Here, we performed anti-dsRNA immunoprecipitation followed by mass spectrometry analysis to fully characterize the dsRNA interactome in Sindbis virus (SINV) infected human cells. Among the identified proteins, we characterized SFPQ (Splicing factor, proline-glutamine rich) as a new dsRNA-associated proviral factor upon SINV infection. We showed that SFPQ depletion reduces SINV infection in human HCT116 and SK-N-BE(2) cells, suggesting that SFPQ may enhance viral production. We demonstrated that the cytoplasmic fraction of SFPQ partially colocalized with viral dsRNAs upon SINV infection. In agreement, we proved that SFPQ association to dsRNA occurs during infection and that SFPQ can bind to the viral genome. Furthermore, we showed that overexpression of a wild-type, but not a mutant deleted in the RNA binding domains, SFPQ increased viral infection. Overall, this study not only represents a compendium of dsRNA-associated factors during viral infection but also identifies SFPQ as a new proviral dsRNA binding protein.

Introduction

Because of their strict dependency on the host cell machinery to replicate, viruses interact with many host factors to ensure the efficient and successful completion of their life cycle. The least complex the viral genome is, the more the virus will rely on cellular proteins. For instance, positive single stranded (ss)RNA viral genomes, which mimic cellular mRNA features, typically encode for a handful of proteins allowing them to replicate and package their genome. As a consequence, these viruses are known to hijack host factors, such as regulatory non-coding RNAs (Damas et al. 2019) as well as several cellular RNA Binding Proteins (RBPs) (Nagy and Pogany 2012; Girardi et al. 2020) causing profound alterations in the cell.

Canonical RBPs participate in every step of virus infection, from the recognition of the viral RNA to its replication and translation (Nagy and Pogany 2012). In particular, a broad range of RNA viruses are able to hijack nuclear shuttling host RBPs and to alter their roles to support their own replication, thereby indirectly impacting host gene expression (Lloyd 2015). Among the most complex interactions between viral RNA and cellular proteins are those needed for the formation of intracellular structures known as 'viral factories', which are not only necessary to allow viral replication, but also to protect the viral genome from detection and clearance by the antiviral response (Novoa et al. 2005). Indeed, to counteract the infection, the cell evolved an arsenal of antiviral factors able to recognize foreign viral features. Thus, the absence of a 5' cap, or the presence of double stranded (ds)RNA structures longer than 30 base pair (bp), will trigger a potent and evolutionary conserved innate immune response. In particular, long viral dsRNA constitutes a universal danger signal in higher eukaryotes, as it accumulates invariably and specifically as a by-product of viral replication or transcription. Antiviral RNA interference (RNAi) constitutes the major antiviral response in plants and invertebrates. It is elicited by recognition and cleavage of long viral dsRNA molecules into small interfering RNAs (siRNA) by the ribonuclease Dicer. SiRNAs are then loaded into effector complexes comprising a member of the Argonaute (Ago) family, where they act as guides to degrade viral RNAs via sequence complementarity and restrict the infection (Guo et al. 2019). The cellular response to viruses can also be triggered by foreign nucleic acids in vertebrates, but it rather culminates with the induction of type I Interferons (IFNs) and of hundreds of interferon-stimulated-genes (ISGs). Such a chain of events perturbs the viral replication but also promotes the inhibition of protein synthesis, cellular RNA degradation and, ultimately, cell death (Stetson and Medzhitov 2006). Several

dsRNA sensors, such as RIG-I, MDA5 or LGP2, and other dsRNA Binding Proteins (dsRBPs) such as PKR, ADAR and OAS proteins have been well characterized so far and their general role during viral infection has been identified (Schlee and Hartmann 2016). Nonetheless, additional cellular factors, such as RNA helicases, are also emerging as general or virus-specific players in the recognition and immune defence to viral dsRNA (Hur 2019). Therefore, the identification of such host factors is crucial to better understand dsRNA sensing in viral infections and to study the interactions between the host and its viruses. In particular, the importance of nuclear proteins in the regulation of innate immune response against cytoplasmic pathogenic RNA molecules remains underexplored. Within the nucleus, paraspeckles are dynamic ribonucleoprotein (RNP) nuclear bodies built by protein liquid-liquid phase transition and defined by the presence of the structural long non-coding (lnc)RNA NEAT1 (nuclear-enriched abundant transcript 1) and the NEAT1-binding paraspeckle proteins SFPQ, NONO (Non-POU domain-containing octamer-binding protein) and PSPC1 (Paraspeckle component 1). Several other proteins and RNAs can be sequestered in these granules resulting either in the inhibition or enhancement of their molecular function (Nakagawa et al. 2018). For instance, hyper-edited RNAs containing Alu inverted repeats (IRAlus) can be specifically retained within nuclear paraspeckles to impair their export and translation.

System-wide approaches to discover the cellular RBP interactome of viral RNA are emerging as key to deepen our understanding of the involvement of host proteins in infected cells (Garcia-Moreno et al. 2018). In particular, many efforts have been made in order to identify host factors able to bind to the viral RNA (LaPointe et al. 2018; Varjak et al. 2013) and to elucidate the role of these factors at different stages of the viral life cycle. Recently, RNA interactome capture (RNA-IC) has also been employed to identify the cellular RNA-binding proteome associated with viral RNA and found out several RBPs which may regulate viral replication and could be targeted to modulate the infection (Garcia-Moreno et al. 2019; Kamel et al. 2021). However, these approaches are focused on genomic or messenger viral RNAs and are not able to reliably identify proteins interacting with replication intermediates, which are one of the key features triggering the cell immune response.

To address this lack of knowledge, we turned to an approach specifically designed to determine the dsRNA-associated proteome during viral infection. As a model for this work, we used Sindbis virus (SINV), which is a member of the alphavirus genus from the *Togaviridae* family. It has a capped and polyadenylated single stranded, positive-sense RNA genome of 12 kb, which consists of two open reading frames (ORFs). ORF1 encodes the non-

structural polyprotein and ORF2 encodes the structural polyprotein. While the structural proteins are translated from a sub-genomic RNA, the non-structural proteins (nsP1, nsP2, nsP3 and nsP4) are directly translated from the genomic RNA since they are necessary for replication of the viral RNA inside the cytoplasm of host cells. This occurs through the synthesis of a complementary antigenomic RNA and the accumulation of long dsRNA intermediates in the cytoplasm of infected cells (Griffin 2007). Here, we describe the determination of the long dsRNA interactome upon SINV infection in human cells in an unbiased manner and characterize the relevance of dsRNA-associated proteins during infection. To do so, we employed a novel approach based on dsRNA immunoprecipitation using a dsRNA-specific antibody followed by proteomic analysis. The outcome of the experiment revealed a number of previously known but also novel factors, among which SFPQ that we validated as a new proviral, dsRNA-associated factor upon SINV infection.

Results

Identification of the dsRNA interactome in mock- and SINV-infected human cells

SINV genomic RNA replicates through the production of a reverse complementary antigenomic RNA (Figure 1A), which results in the accumulation of long dsRNA intermediates in the cytoplasm of infected cells. In order to characterize the long dsRNA interactome in mock and SINV infected human colon carcinoma HCT116 cells, we adapted the method of immunoprecipitation of long RNA duplexes (Dhir et al. 2018) using the anti-dsRNA (J2) antibody, which specifically recognizes dsRNAs longer than 40 bp (Schonborn et al. 1991; Bonin et al. 2000), to identify dsRNA-associated proteins. The experimental design was based on the pull-down of long dsRNA molecules from cellular lysates of HCT116 cells infected with SINV-GFP for 24 h at a MOI of 0.1, or mock-infected. Since we combined the anti-J2 DsRNA Immunoprecipitation to Mass Spectrometry of the isolated dsRNA-associated protein complexes, we named this approach DRIMS (Figure 1B). In order to validate the enrichment of long dsRNA molecules in SINV-infected IP conditions we performed dot blot analysis using the J2-antibody. We observed a specific signal both in total RNA (INPUT) and J2-IP upon SINV infection compared to the IgG-IP, suggesting that the dsRNA species accumulate in infected cells and were immunoprecipitated by DRIMS (Figure 1C). The presence of viral RNA specifically immunoprecipitated in the infected samples was also assessed by RT-qPCR on RNA extracted from the J2- and control IgG -IP (Figure 1D).

Protein profiles in total extracts, J2 and IgG eluates were analysed by silver staining of polyacrylamide gels (Figure S1A) and proteins immunoprecipitated in the J2- and IgG-IP samples were then analysed by liquid chromatography coupled to tandem mass spectrometry (LC-MS/MS). After identification of viral and human proteins in each sample, hierarchical clustering analysis of the J2-IP replicates identified two distinct groups, indicating higher similarities in the protein profiles among the mock and SINV samples, respectively (Figure S1B). Differential expression analysis was then performed by comparing J2-IP samples in SINV-infected *versus* mock-infected cells and revealed the enrichment of both host and viral proteins upon viral infection (Figure 2A and Table S1). Protein enrichment of the J2-IP over the IgG-IP samples upon SINV-GFP infection showed enrichment profiles similar to SINV J2-IP versus mock J2-IP ones (Figure S1C), while comparison of the J2-IP to IgG-IP samples in mock conditions revealed few significantly enriched proteins, potentially associated to endogenous dsRNAs (Figure S1D).

We identified a total of 63 (6 viral and 57 cellular) proteins significantly enriched in SINV-infected J2-IP samples compared to mock, validated with an FDR<1%, having at least 5 spectral counts in the most abundant condition, a fold change of at least 2 and an adjusted p-value lower than 0.05 (Table S1). As expected, viral non-structural proteins which are necessary for SINV replication were specifically enriched in the SINV J2-IP compared to the mock J2-IP (Figure 2A). In addition, capsid, E1 and E2 structural proteins were also immunoprecipitated. Gene Ontology (GO) term enrichment analysis of the cellular overrepresented proteins in SINV J2-IP samples based on molecular function, cellular components and biological processes indicated that most of these proteins are RNA binding proteins (RBPs) (Figure S1E, left panel), present in both cytoplasmic and nuclear ribonucleoprotein granules (Figure S1E, middle panel) and are involved in pre-mRNA processing/metabolism (Figure S1E, right panel).

Moreover, STRING analysis showed that these enriched cellular proteins mostly belong to known interaction networks (Figure 2B). Among the most enriched cellular proteins in infected conditions, 11 have InterPro-annotated dsRNA binding domains and are known to be involved in antiviral innate immunity to long dsRNAs, such as ADAR1 (also known as DSRAD), ADARB1, PKR (also known as E2AK2), PACT (also known as PRKRA), TARBP2 (also known as TRBP) (Hur 2019), STAU1 (Wickham et al. 1999), STRBP (Coolidge 2000), and ILF3 (Watson et al. 2019) (Figure 2A-B). We also retrieved several RBPs previously described as having a role in SINV infection such as G3BP1 and G3BP2 (Cristea et al. 2010), which localize to stress granules, or HNRNPA1 (Lin et al. 2009), which relocalizes to the cytoplasm upon infection and enhances SINV translation. Many other RBPs not yet identified in the context of SINV infection were enriched in the SINV J2-IP, such as PNPT1 (Dhir et al. 2018), FXR1 (Fragile X-related protein-1), ZFR (Zinc finger RNA-binding protein), TRA2B (Transformer 2 Beta Homolog), SRRM2 (Serine/Arginine Repetitive Matrix 2), SRSF6 (Serine And Arginine Rich Splicing Factor 6), RBMX (RNA-binding motif protein X-chromosome, also known as HNRNPG), KHDRBS1 (KH RNA Binding Domain Containing, Signal Transduction Associated 1), IGF2BP3 (Insulin Like Growth Factor 2 mRNA Binding Protein 3) or BCLAF (Bcl-2 Associated Transcription Factor 1). Among the dsRNA associated factors identified upon SINV infection, we also found several RNA helicases such as DHX9 (DExH-Box Helicase 9), DDX5 (DEAD-Box Helicase 5), DDX30 (DExH-Box Helicase 30), DDX3X (DEAD-Box Helicase 3 X-Linked), UPF1 (UPF1 RNA Helicase and ATPase) and MOV10 (Mov10 RISC Complex RNA Helicase). Interestingly, we also identified DICER as specifically associated to dsRNAs upon

SINV infection. Since the J2-Ab was previously shown to be unable to recognize pre-miRNA structures (White et al. 2014), this indicates a potential role of DICER in the recognition of long dsRNAs in infected human cells (Figure 2A-B).

In addition, several nuclear RBPs known to be involved in paraspeckle formation, such as NONO/p54nrb, SFPQ/PSF, RBM14, PSPC1 and MATR3 (Nakagawa et al. 2018), showed a 1.5 to 5 log2 fold change enrichment in the SINV J2-IP compared to the mock J2-IP (Figure 2A-B). In particular, NONO and SFPQ were already present in mock J2-IP samples and their association with long dsRNA seemed to increase upon infection suggesting that they could associate with either viral or virus-induced host RNAs (Table S1).

Next, we performed western blot analyses on J2-IP and IgG-IP samples in mock and SINV-infected conditions to validate some of the enriched proteins identified by mass spectrometry. We confirmed an increased association of PACT, PKR, ADAR1, DHX9 and MATR3 with dsRNA upon SINV infection (Figure 2C). We also validated the presence of DICER in the J2-IP only in virus-infected cells, which strengthens the potential involvement of this factor in the response to viruses in our experimental setup. Finally, we also validate SFPQ as a dsRNA-enriched protein retrieved in SINV-infected cells (Figure 2C).

Overall, our data suggest that the DRIMS approach is a powerful way to identify long dsRNA interactome upon viral infection in human cells and that beside known antiviral factors it allowed us to isolate several novel RBPs potentially involved in dsRNA recognition, which may affect SINV infection.

SFPQ depletion reduces SINV infection in HCT116 and SK-N-BE(2) cells

In order to further decipher the involvement of the factors enriched with dsRNA upon SINV infection by DRIMS, we performed an siRNA-based loss-of-function analysis on 37 candidates in HCT116 cells and quantified the effect of specific gene depletion on SINV-GFP infection compared to the siCTRL condition by measuring GFP fluorescence intensity. As functional controls, we transfected either siRNAs directly targeting the viral 3'UTR (siSINV) (López et al. 2020) or siRNA targeting the antiviral protein PKR (siPKR) (Figure 3A, blue and red bars, respectively). We observed that knock-down (KD) of either DDX5 or SFPQ significantly reduces GFP expression in HCT116 infected cells compared to siCTRL (Figure 3A, black bars). Since the RNA helicase DDX5 is already known to bind dsRNAs and its role in viral infection has already been extensively proven so far (Cheng et al. 2018), we chose to pursue the functional characterisation of SFPQ in terms of dsRNA association and impact on SINV infection. In agreement with the decrease in GFP, the levels of viral

capsid protein (Figure 3B), viral titers (Figure 3C) and viral genomic RNA (Figure 3D) were reduced upon *SFPQ* KD compared to the control (siCTRL). We validated these findings in another cell type suitable for SINV infection, namely the SK-N-BE(2) human neuroblastoma cells, which can be differentiated into neurons upon retinoic acid (RA) treatment (Figure S2). We observed not only the decrease in GFP by epifluorescence microscopy (Figure S2A), but also a reduction in the levels of viral capsid (Figure S2B) and viral titers (Figure S2C) upon *SFPQ* KD compared to the control (siCTRL).

To validate the effect of SFPQ KD on SINV infection by an independent approach, we generated a heterozygous (+/-) *SFPQ* knock-out HCT116 cell line by CRISPR/Cas9 (Figure 4A-B). We did not manage to retrieve a homozygous KO cell line, probably due to the importance of SFPQ in cell viability (Yarosh et al. 2015). Despite the presence of one wild-type allele, we could functionally validate the negative impact of SFPQ reduction on GFP expression levels (Figure 4C), capsid protein levels (Figure 4D), and viral titers (Figure 4E), in SFPQ +/- cells compared to WT HCT116 cells.

Overall, our results demonstrate a functional effect of SFPQ depletion on SINV infection in two independent cell types and with two different loss-of function methods, suggesting that SFPQ could play a proviral role during infection.

SFPQ binds to cytoplasmic dsRNA upon SINV infection, and its RNA binding capacity is important for the proviral effect

The functional effect observed on SINV infection upon SFPQ depletion could be both dependent and independent of SFPQ direct association to dsRNAs in the cytoplasm. Hence, we verified the SFPQ localization before and after SINV infection by immunofluorescence analysis (Figure 5A). As a control, the presence of long dsRNAs was observed in HCT116 cells infected with SINV for 24 h at an MOI of 0.1 compared to uninfected ones using the anti-dsRNA (J2) antibody. Since SFPQ can interact with NONO within the paraspeckles, we also checked NONO subcellular localization and observed a nuclear accumulation in discrete foci whose intensity increased upon infection consistent with a change in paraspeckles induced by SINV in HCT116 cells. We also tested the localization of G3BP1, which was immunoprecipitated together with dsRNAs by DRIMS upon infection and is known to be present in SINV-induced cytoplasmic stress granules (Cristea et al. 2010). SFPQ mostly localized to the nucleus but could also accumulate in the cytoplasm in both mock and infected cells (Figure 5A). A similar SFPQ protein subcellular accumulation profile before and after infection was also validated by nuclear/cytoplasmic fractionation experiments

(Figure 5B). Nonetheless, the presence of discrete cytoplasmic SFPQ foci induced upon SINV infection suggested a change in the protein distribution within the cytoplasmic compartment specifically in the presence of the virus (Figure 5A, lower panel). We then performed co-immunofluorescence analysis to verify whether SFPQ could associate to long dsRNAs in the cytoplasm upon infection. We could observe that the cytoplasmic SFPQ moiety partially colocalizes (Pearson's coefficient = 0.5) with the J2 signal in infected cells (Figure 5C).

To further characterize the SFPQ-dsRNA interaction, we immunoprecipitated the endogenous SFPQ protein in mock and SINV infected HCT116 cells and isolated the associated RNAs (RNA-immunoprecipitation, RIP). After verifying the SFPQ immunoprecipitation by western blot analysis (Figure 6A), we performed a dot blot analysis on immunoprecipitated RNAs using the J2-antibody to visualize long dsRNA molecules (Figure 6B). While uninfected cells did not show any dsRNA accumulation, we observed a specific signal both in total RNA (INPUT) and SFPQ-IP upon SINV infection compared to the control IgG-IP, suggesting that the association of dsRNA species with SFPQ takes place in infected cells. These data correlate with the SFPQ enrichment on dsRNAs upon SINV infection observed by DRIMS (Figure 2A-B, Table S1) and validated by western blot (Figure 2C). Additionally, we demonstrated by RT-qPCR that the viral genomic RNA is specifically enriched in the SFPQ-RIP compared to the IgG-RIP (Figure 6C) supporting the fact that among the dsRNAs associated to SFPQ there are those of viral origin.

To rule out that SFPQ association to dsRNAs is solely mediated by its binding to flanking single stranded (ss)RNA regions, we performed J2-IP experiments followed by on-beads RNase T1 treatment (Figure S3). We could confirm the efficiency of RNAse T1 digestion on total RNA (INPUT) (Figure S3A) and that the association of PKR (dsRBP, positive control) was unchanged before and after treatment, while Ago2 was not enriched (ssRBP, negative control). Interestingly, enrichment of SFPQ in the J2-IP upon infection remained unchanged before and after RNase T1 digestion, suggesting a direct binding to dsRNA regions in infected cells (Figure S3B). To assess whether the effect of SFPQ on SINV infection depends on its RNA binding capacity, we performed rescue experiments in SFPQ+/- cells and tested the effect on SINV infection upon overexpression of either a wild-type version of SFPQ or a SFPQ mutant deleted of both RNA Recognition Motifs (Knott et al. 2016) (SFPQ ΔRRM1-2) (Figure 6D). We observed an increase of both GFP and capsid proteins and up to 6-fold increase in viral production upon WT SFPQ overexpression (Figure 6E-G). We could also

observe a decrease of both viral protein accumulation and viral titer upon expression of SFPQ ΔRRM1-2 compared to the WT SFPQ (Figure 6E-G), suggesting that the RNA binding is important but not essential for the proviral activity. Overall, these findings indicate that SFPQ is able to bind dsRNA upon infection, that the interaction takes place in the cytoplasm where the viral RNA replicates and the proviral effect partially depends on SFPQ RNA binding domains.

Discussion

Unbiased proteome-wide approaches have proven to be very useful to find new host factors regulated by or able to regulate viral infections. Over 2000 cellular RBPs have been described so far (Hentze et al. 2018), but understanding which RBP participates to the life cycle of a virus and at which step remains a challenge. To date, there has been little(Incarbone et al. 2021) to no reports of the identification of proteins binding specifically to viral replication intermediates. A recent affinity proteomics approach using different synthetic nucleic acids identified novel conserved proteins able to associate to dsRNAs (Pennemann et al. 2021), but the whole picture of the viral dsRNA-associated proteome *in vivo* remains to be assessed. Here, we showed that our DRIMS approach is very effective to identify dsRNA associated proteins, since it allowed us to validate the presence of proteins with canonical dsRNA binding domains (dsRBDs) or helicase domains (Hur 2019) involved in antiviral innate immunity, such as PKR, PACT, Staufen, ILF2, ILF3 and DHX9 associated to long dsRNAs upon SINV infection in human cells. Interestingly, we also identified factors such as DICER or ADAR1, suggesting that SINV viral RNA duplexes are a potential target for enzymes acting on dsRNA, although we did not test the functionality of these interactions. We recently showed that DICER could interact with PKR upon SINV infection and could potentially down-regulate its function (Montavon et al. 2021). The fact that we found it enriched by our DRIMS approach further confirms the importance of DICER in modulating dsRNA-based innate immunity in an RLR-like manner. We also identified non canonical RBPs, which is not surprising given that increasing evidences show that host factors without typical protein domains known to bind to ss or dsRNA are still able to associate with foreign nucleic acids and act as RNA co-sensors by modulating canonical dsRNA sensor activity(Liu and Gack 2020). For instance, several hnRNP family members can negatively regulate RLR signaling. Upon viral infection, HNRNPE2 translocates from the nucleus to the cytoplasm where it interacts with MAVS to mediate its degradation (You et

al. 2009). HNRNPM, which shuttles as well from the nucleus to the cytoplasm in infected cells, impairs the RNA-binding activity of RLRs (Cao et al. 2019). Finally, HNRNPC protects cells from accumulating RIG-I-stimulatory endogenous *Alu*-rich dsRNA (Wu et al. 2018).

Surprisingly, we were not able to find expected innate immune dsRNA sensors of the RIG-I like receptor (RLR) family, such as RIG-I or MDA5 using our approach. One hypothesis could be that their association to the substrate is too stable and does not allow the J2-antibody to recognize and isolate the long dsRNA. Alternatively, a relativly low concentration of RIG-I and MDA5 (Akhrymuk et al. 2016) may explain why they would not represent preponderant actors in the recognition of SINV dsRNA compared to other factors such as PKR in the cellular context used here. We did however isolate all four viral nsPs in SINV-infected cells suggesting that the DRIMS approach is suitable for the isolation of proteins bound to the replication complex itself.

Alphavirus infection strongly affects many cellular pathways to favour viral production and interfere with the antiviral response. For instance, arthritogenic alphavirus nsP3 protein has been shown to interact with and modulate the activity of proteins related to stress granule formation, such as G3BP1. Proteomic studies performed to characterize the protein complexes associated with the SINV viral protein nsP3 (Frolova et al. 2006) or the RNA-dependent RNA polymerase nsP4 (Cristea et al. 2010) assessed that the interaction with G3BP1 and G3BP2 is important for the formation and function of SINV RNA genome replication complexes. Accordingly, among the proteins isolated by DRIMS, we did enrich for stress granules related factors. During viral infection, stress granules recruit numerous antiviral proteins including RIG-I or PKR and enhance the induction of the innate immune response and viral resistance (Protter and Parker 2016). Proteins from stress granules such as G3BP1 are also able to directly bind to viral dsRNA (Kim et al. 2019). Although the replication proceeds in the cytoplasm of infected cells and does not directly depend on nuclei, this family of viruses has the ability to alter subcellular localization of host nuclear RBPs (Lloyd 2015) and old world alphaviruses' nsP2 protein has been shown to inhibit RNA polymerase II transcription (Akhrymuk et al. 2012). The abundance of nuclear proteins isolated with our approach, many of which with a known localization within paraspeckles, suggested that some of these factors may also localize to the cytoplasm upon SINV infection to favour or inhibit the viral cycle and possibly modulate the innate immune response. Due to their distinct localisation, nuclear and cytoplasmic RNP granules have long been considered independent entities. Recently, a crosstalk between stress granules and paraspeckles has been

proposed in which stress granules would act as positive regulators of nuclear RNP granule assembly in response to stress. In particular, an overlap between the proteomes of paraspeckles and stress granules has been observed and it suggests that cytoplasmic granule formation may regulate paraspeckle assembly via sequestration or release of specific proteins (An et al. 2019; An and Shelkovnikova 2019).

For all these reasons, we focused our attention on the paraspeckle component SFPQ, which despite its main nuclear localization may also have important non-nuclear functions such as mRNA post-transcriptional regulation and RNA granule formation especially in neurons (Lim et al. 2020). Beside its localization within paraspeckles as a heterodimer with NONO (Knott et al. 2016), SFPQ is an ubiquitous multifunctional protein involved in many aspects of nucleic acid biology in the nucleus, ranging from genome stability to transcription, as well as pre-mRNA splicing, localization and 3'end RNA processing (Yarosh et al. 2015). Thus, SFPQ is known to bind to single stranded RNA and more particularly to the poly-pyrimidine tract upstream of intronic 3'splice site (ss) in cellular pre-mRNAs(Gil et al. 1991; Patton et al. 1991) to assist spliceosome assembly, but also to C-rich sequences close to the 5′ splice sites of long introns therefore regulating long intron-containing gene expression (Iida et al. 2020). In addition to its involvement in multiple cellular processes, SFPQ has also been reported to play a role in the regulation of several RNA viruses (Yarosh et al. 2015). For instance SFPQ interacts with HIV viral RNA and favours its nuclear-cytoplasmic export (Kula et al. 2013), and it also increases the efficiency of influenza virus mRNA polyadenylation (Landeras-Bueno et al. 2011). Moreover, SFPQ proviral effect has been reported during Hepatitis delta virus (HDV) (Greco-Stewart et al. 2006), human rhinovirus A16 (HRV16) (Flather et al. 2018), encephalomyocarditis virus (EMCV) (Zhou et al. 2019) and Severe acute respiratory syndrome coronavirus 2 (SARS-CoV-2) (Labeau et al. 2022)infections. Accordingly, we demonstrated that SFPQ expression has a significant impact on SINV infection, since SFPQ knock-down causes a reduction in SINV protein levels as well as in viral production. This phenotype was reproducible in two independent cell types (HCT116 and SK-N-BE(2) cells) and in SFPQ +/- knockout (+/- KO) cells, suggesting a proviral role for SFPQ during SINV infection. It is worth to mention that *SFPQ* seems to be an essential gene (Yarosh et al. 2015), which could explain why we were not able to generate a homozygous knock-out cell line. We also assessed SFPQ localization before and after SINV infection in HCT116 cells by immunofluorescence, and observed that its accumulation occurs both in the nucleus and in the cytoplasm, which was compatible with its association with viral RNA upon infection.

Our rescue experiments correlate with a proviral function of SFPQ upon SINV infection. Interestingly, a recent study revealed a direct role of SFPQ on antiviral innate immunity showing that paraspeckle proteins may couple both transcription and post-transcriptional events. Indeed, SFPQ acts as a transcriptional repressor on the promoter of certain immune related genes and its re-localization to the core of paraspeckles upon infection leads to the induction of the antiviral gene program (Imamura et al. 2014). However, our data indicate that such a positive effect partially depends on the SFPQ RNA binding capacity and to our knowledge, a direct link between paraspeckle proteins and their binding to viral dsRNA has not been investigated so far. Our data also indicate that NONO depletion does not affect viral infection, suggesting that SFPQ proviral function could be independent on its paraspeckle cofactor. Moreover, NONO specifically localizes in the nucleus before and after SINV infection, while a fraction of SFPQ accumulates in the cytoplasm. The SFPQ/NONO complex is well known to bind to edited cellular dsRNA in the nucleus via NONO interaction with the nucleic acids (Zhang and Carmichael 2001). Whether the dsRNA bound by SFPQ upon infection is specifically the viral replication intermediate or whether it is of cellular origin remains to be assessed. Indeed, we cannot exclude that host dsRNA accumulation specifically occurs in response to viral stress. As paraspeckles are involved in nuclear retention of edited transcripts containing dsRNA structures, it is tempting to imagine that binding of SFPQ to SINV RNA in the cytoplasm could change paraspeckles composition and indirectly affect localization and expression of certain genes upon infection.

Materials and Methods

Cell culture, viral stocks and virus infection

Cell lines were maintained at 37°C in a humidified atmosphere containing 5% CO_2. HCT116, BHK-21 and Vero cells were cultured in Dulbecco's Modified Eagle medium (DMEM; Invitrogen) supplemented with 10% FBS. SK-N-BE(2) cells (95011815, Sigma-Aldrich) were maintained in 1:1 medium composed of Ham's F12 medium (Gibco, Thermo Fisher Scientific Inc.) supplemented with 15% FBS and Eagle's Minimal Essential Medium (ENEM) supplemented with 1% NEAA (Gibco, Thermo Fisher Scientific Inc.). SK-N-BE(2) cell differentiation was induced by 10 µM retinoic acid (RA) treatment (R2625, Sigma-Aldrich) for 5 days. Plasmids carrying a green fluorescent protein (GFP)-SINV genomic sequence or wild-type SINV genomic sequence (kindly provided by Dr Carla Saleh, Institut Pasteur, Paris, France) were linearized and used as a substrate for *in vitro* transcription using mMESSAGE mMACHINE capped RNA transcription kit (Ambion, Thermo Fisher Scientific Inc.) as in (López et al. 2020). Viral stocks were prepared in BHK-21 baby hamster kidney cells, and titers were measured by plaque assay in Vero cells. Cells were infected at a MOI of 10^{-1} and samples were harvested at 24 hours post-infection (hpi) unless specified otherwise.

Standard plaque assay

Vero cells seeded either in 96- or 24-well plates were infected with viral supernatants prepared in cascade 10-fold dilutions for 1 h. Afterwards, the inoculum was removed and cells were cultured in 2.5% carboxymethyl cellulose for 72 h at 37ºC in a humidified atmosphere of 5% CO2. Plaques were counted manually under the microscope. For plaque visualization, the medium was removed, cells were fixed with 4% formaldehyde for 20 min and stained with 1x crystal violet solution (2% crystal violet (Sigma-Aldrich), 20% ethanol, 4% formaldehyde).

DsRNA Immunoprecipitation and Mass Spectrometry (DRIMS)

Protein G Dynabeads were washed and resuspended in FA lysis buffer (1mM EDTA [pH 8.0], 50 mM HEPES-KOH [pH 7.5], 140 mM NaCl, 0.1% sodium deoxycholate (w/v), 1% triton X-100 (v/v), 1X protease inhibitors). Two micrograms (µg) of mouse anti-dsRNA J2 (SCICONS) or mouse anti-IgG (Cell signalling) were bound to 50 µL of beads for 1 h at room temperature. 80–90% confluent HCT116 cells in 10 cm^2 plate were washed with cold

PBS. Cells were scraped, transferred to a falcon and spin at 1000 rpm at 4°C for 5 min. For each IP, cell pellet from one 10 cm^2 plate was lysed in 100 µL of Nuclei lysis buffer (50 mM Tris–HCl [pH 8.1], 10 mM EDTA [pH 8.0], 1% sodium dodecyl sulphate (SDS) (w/v), 1X protease inhibitor), incubated on ice for 10 min and diluted ten-fold with FA lysis buffer containing RNase inhibitor. Samples were sonicated in a BioRuptor (Diagenode) on high ("H") for 5 min with 30 s on/off cycles. Following a spin at 13,000 rpm at 4°C for 5 min, supernatant was carefully transferred to a new tube and 40 µL of the volume were kept as input lysate. After 1 hour of pre-clearing at 4°C with yeast tRNA-blocked Protein G Dynabeads, Ab conjugated beads (50 µL) were added to the lysate and incubated for 2-3 hours at 4°C. Following magnetic separation, beads were washed twice with 1 mL of FA lysis buffer and twice with 1 mL of TE buffer (EDTA (10 mM, [pH 8.0]), Tris–HCl (100 mM, [pH 8.0]). Beads were incubated 10 min at 95°C with 40 µL 2X SDS Laemmli loading buffer (120 mM Tris/HCl [pH 6.8]; 20% glycerol; 4% SDS, 0.04% bromophenol blue; 10% β-mercaptoethanol) and proteins were analysed either by western blot or by silver staining after electrophoretic separation on polyacrylamide SDS-PAGE gel (Bio-Rad 4–20% Criterion™ TGX Stain-Free™ Protein Gel, 18 well, #5678094) using the SilverQuest™ Silver Staining Kit (ThermoFisher Scientific #LC6070) according to the manufacturer's instructions.

For mass spectrometry experiments, proteins eluted from the beads were precipitated overnight with methanol containing 0.1% ammonium acetate and digested with trypsin after reduction and alkylation steps. Generated peptides were analysed by nanoLC-MS/MS on a QExactive□+□mass spectrometer coupled to an EASY-nanoLC-1000 (Thermo-Fisher Scientific, USA). The data were searched against a database containing the Human swissprot sequences (2017_01), the SINV and GFP sequences with a decoy strategy. Peptides were identified with Mascot algorithm (version 2.5, Matrix Science, London, UK), and the data were imported into Proline 1.4 software [http://proline.profiproteomics.fr/]. The protein identifications were validated using the following settings: Mascot pretty rank□<□=□1, FDR□<□=□1% for PSM scores, FDR□<□=□1% for protein set scores. The total number of MS/MS fragmentation spectra was used to quantify each protein from three independent replicates.

Mass spectrometry data obtained for each sample, including the proteins identified by the Proline software suite and their associated spectral counts (SpC), were stored in a local MongoDB database and subsequently analysed through a Shiny Application built upon the R

packages msmsEDA (Gregori J, Sanchez A, Villanueva J (2014). msmsEDA: Exploratory Data Analysis of LC-MS/MS data by spectral counts. R/Bioconductor package version 1.22.0) and msmsTests (Gregori J, Sanchez A, Villanueva J (2013). msmsTests: LC-MS/MS Differential Expression Tests. R/Bioconductor package version 1.22.0). Exploratory data analyses of LC-MS/MS data were thus conducted and differential expression tests were performed using a negative binomial regression model. The p-values were adjusted with FDR control by the Benjamini-Hochberg method and the following criteria were used to define differentially expressed proteins: an adjusted p-value < 0.05, a minimum of 5 SpC in the most abundant condition, and a minimum Log2 fold change of 1. GO term analysis was performed using the EnrichR web-based tool (http://amp.pharm.mssm.edu/Enrichr) (Chen et al. 2013; Kuleshov et al. 2016). The direct interaction network for the enriched proteins was generated with the Cytoscape StringApp (Doncheva et al. 2019).

SFPQ RNA Immunoprecipitation

Four million of either mock or SINV-infected HCT116 cells (MOI 0.1) were lysed 24 h post-infection using RIP immunoprecipitation buffer (50 mM Tris-HCl [pH 7.5], 150 mM NaCl, 5 mM EDTA, 0.05% SDS, 1% triton, 1 tablet of commercial protease inhibitor cocktail (Sigma Aldrich)). Lysates were treated for 20 min at 37°C with 1 µL of RNase-free DNase I by adjusting final concentration of $MgCl_2$ (10 mM) and $CaCl_2$ (5 mM). 1 µL of RNase inhibitor (Ribolock, ThermoFisher Scientific) was also added.

Lysates were cleared by maximal centrifugation 10 min at 4°C. Supernatants were transferred in new Eppendorf tubes. Lysates were then precleared 1 h at room temperature with magnetic bead treated with tRNA solution (RIP buffer + 10 nM of tRNA).

The lysates were incubated overnight with RIP immunoprecipitation buffer containing magnetic Protein G beads conjugated with human SFPQ/PSF antibody (sc-271796, Santa Cruz, Cliniscience) or negative control mouse IgG (5415S, Cell signalling, Ozyme).

Beads were washed 3 times with RIP immunoprecipitation buffer, 3 times with wash buffer (50 mM Tris-HCl [pH 7.5], 200 mM NaCl, 5 mM EDTA, 0.05% SDS, 1% triton, 1 tablet of commercial protease inhibitor cocktail (Sigma Aldrich)) and twice with cold PBS 1X.

Immunoprecipitated RNAs and proteins were isolated by TRIzol Reagent (Invitrogen) or Laemmli loading buffer, respectively. Extracted RNAs were analysed by RT-qPCR and proteins were analysed by western blot.

Subcellular fractionation

HCT116 cells infected by SINV during 24hrs at MOI 0.1 or mock cells were washed with cold PBS 1X and gently resuspended in 3mL of hypotonic buffer (10 mM HEPES [pH 7.9], 1,5 mM $MgCl_2$, 10 mM KCl, 1 tablet of commercial protease inhibitor cocktail (Sigma Aldrich)) and incubated on ice for 2 min. NP40 (0.4% final concentration) was added on the cell suspension. Cytoplasmic and nuclear fraction were separated by a centrifugation step at 500g. The cytoplasmic fraction was removed and kept at 4°C. The nuclear pellet was washed by 3 times centrifugation steps (2 min at 500g) with hypotonic buffer. The nuclear pellet was resuspended in 1 mL of lysis buffer (20 mM tris-HCl [pH 8.0], 100 mM KCl, 10 mM KCl, 0.2 mM EDTA, 0.5 mM DTT, 5% glycerol and 1 tablet of commercial protease inhibitor cocktail (Sigma Aldrich).

Western blotting

For protein analysis in total lysates and IP, proteins were extracted by collecting cell lysates in RIPA buffer (50 mM Tris-HCl [pH 7.5], 150 mM NaCl, 5 mM EDTA, 0.05% SDS, 1% triton, 1 tablet of commercial protease inhibitor cocktail (Sigma Aldrich)). Lysates were cleared by centrifugation at 13000 rpm for 30 min at 4°C to remove cell debris and the supernatant was retained for western blotting. According to the experiment, 20 µg of proteins of each sample or both input and eluates from the IPs were heated in Laemmli loading buffer at 95°C for 5 min and loaded on a SDS-polyacrylamide electrophoresis gel (Bio-Rad 4–20% Mini-PROTEAN® TGX Stain-Free™ Protein Gels, 10 well, #4568093). Proteins were transferred to a nitrocellulose membrane by wet transfer in 1x Tris-Glycine + 20% ethanol buffer. Membranes were blocked in 5% milk and probed with the antibodies indicated below (between 1:200 and 1:5000). Viral proteins were detected using primary polyclonal antibodies against SINV capsid or nsP2 (kind gift from Dr Diane Griffin, Johns Hopkins University School of Medicine, Baltimore, MD). Anti-mouse-HRP (NXA931, GE Healthcare Thermo Fisher Scientific Inc.) or anti-rabbit-HRP (NA9340, GE Healthcare, Thermo Fisher Scientific Inc.) secondary antibodies were used (1:10000). Detection was performed using SuperSignal West Femto Maximum Sensitivity Substrate (Pierce, ThermoFisher Scientific) and visualized on a Fusion FX imaging system (Vilber).

Immunostaining

HCT116 cells were plated on Millicell EZ 8-well slide (Merck Millipore) (60 000 cells/well) and fixed with 4% formaldehyde (Sigma Aldrich), diluted in PBS 1X for 10 min at room

temperature and incubated in blocking buffer (0.1% Triton X-100; PBS 1 X; 5% normal goat serum) for 1 h. Primary antibodies (see list below) were diluted in blocking buffer between 1:200 and 1:000 and incubated overnight at 4°C. Between each step, cells were washed with PBS 1X-Triton 0.1%. Cells were then incubated 1 h at room temperature with either goat anti-mouse Alexa 594 (A11032, Invitrogen) or goat anti-rabbit Alexa 488 (A11008, Invitrogen) secondary antibodies diluted at 1:1000 in PBS 1X-Triton X-100 0.1%. Cell nuclei were stained with DAPI (Life Technologies, Thermo Fisher Scientific) diluted at 1:5000 in PBS 1X during 5 min. Slides were mounted with coverslip with Fluoromount-G mounting media (Southern Biotech) and observed by confocal microscopy (LSM780, Zeiss).

Antibodies

NAME	species	ref	provider
J2	mouse	J2	SCICONS English and Scientific Consulting Kft, Hungary
PKR human	rabbit	ab32506	Abcam
SFPQ/PSF	rabbit	ab39148	Abcam
SFPQ/PSF	mouse	sc-271796	Santa Cruz
NONO	mouse	sc-166702	Santa Cruz
MATRIN3	mouse	sc-81318	Santa Cruz
PACT	rabbit	ab75749	Abcam
Histone H3	rabbit	ab1791	Abcam
PSPC1	mouse	sc-374181	Santa Cruz
ADAR1	mouse	sc-271854	Santa Cruz
IgG	mouse	5415S	Cell signalling
hNRNPA1	mouse	sc-32301	Santa Cruz
TUBULIN	mouse	T6557	Sigma-Aldrich
myc	mouse	ab32	Abcam
GAPDH-HRP	mouse	ab9482	Abcam

RNA extraction and RT-qPCR

Total and immunoprecipitated RNAs were extracted using Tri-Reagent (Invitrogen, Fisher Scientific) according to the manufacturer's instructions. For total RNA, 1 µg of RNA was reverse transcribed using SuperScript IV Vilo (Invitrogen, #11756050) according to the manufacturer's instructions.

Real-time-PCR was performed with Maxima SYBR Green qPCR Master Mix (Applied Biosystem, #4309155) at an annealing temperature of 60°C on a CFX96 touch Real-Time PCR machine (Biorad) using the following primers:

SINV genome FW: 5'-CCACTACGCAAGCAGAGACG-3';

SINV genome RV: 5'-AGTGCCCAGGGCCTGTGTCCG-3';

GAPDH FW: 5'-CTTTGGTATCGTGGAAGGACT-3';

GAPDH RV: 5'-CCAGTGAGCTTCCCGTTCAG- 3'.

SiRNA transfection

Transfection complexes were prepared using ON-TARGETplus Human siRNA (Horizon), siRNAs against ADAR (L-008630-00), BCLAF1 (L-020734-00), CSNK2A1 (L-003475-00), DDX3X (L-006874-02), DDX5 (L-003774-00), DHX15 (L-011250-01), DHX30 (L-017196-01), DHX9 (L-009950-00), DICER1 (L-003483-00), ELAV1 (L-016006-00), FASN (L-003954-00), FUS (L-009497-00), G3BP1 (L-012099-00), G3BP2 (L-015329-01), HNRNPA1 (L-008221-00), HNRNPL (L-011293-01), HNRNPQ/ SYNCRIP (L-016218-00), IGF2BP2 (L-017705-00) ILF3 (L-012442-00), MATR3 (L-017382-00-0005), NONO (L-007756-01-0005), PACT/ PRKRA (L-006426-00), PARP1 (L-006656-03), PNPT1 (L-019454-01), PSPC1 (L-020596-01-0005), RBM14 (L-020144-00-0005), SFPQ (L-006455-00-0005), SRSF1 (L-018672-01), STAU1 (L-011894-00), STRBP (L-015439-02), TARBP2 (:L-017430-00-0005), THRAP3 (L-019907-00), YBX1 (L-010213-00), YTHDF2 (L-021009-02), ZFR (L-019266-01), PKR (L-003527-00-0005), PKR/EIF2AK2 (L-003527-00-0005), non-targeting Control Pool (D-001810-10-05) or siRNA against SINV 3'UTR (Integrated DNA Technologies) (López et al. 2020) at a final concentration of 50 nM and Lipofectamine 2000 transfection reagent (Thermo Fisher Scientific, #11668019) diluted in Opti-MEM transfection medium according to the manufacturer's instructions and they were added to 20 000 HCT116 cells in 96 well plates. Two days post-transfection, cells were subjected to SINV-GFP viral infection at MOI 10^{-1} for 24 hours before fixation and staining with Hoechst 3342 (labelling the nucleus). GFP quantification was carried out with the INCell Analyzer

1000 Cellular Imaging and Analysis System (GE Healthcare).

Alternatively, 600 000 HCT116 cells were reverse transfected with 20 nM siRNA SFPQ or CTRL in 6-well plates, then transfected again 24 hours later and subsequently incubated for 24 hours before being infected with SINV-GFP at MOI 10^{-1} for 24 hours. For knock-down experiments in SK-N-BE(2) cells, 20000 cells were first transfected with 50 nM of siRNA specific to SFPQ or CTRL in 6-well plates and 6 hours later, differentiation was induced by 10 µM retinoic acid (RA) treatment (R2625, Sigma-Aldrich). Samples were then analysed by epifluorescence microscopy, western blot, RT-qPCR or plaque assay.

SFPQ CRISPR/Cas9 knock-out

Guide RNA (gRNA) sequences targeting human SFPQ were designed using the CRISPOR tool (http://crispor.tefor.net) and cloned into pX459-V2 vector (Addgene Plasmid #62988). Briefly, 100 ng of digested vector and 0.25 µM of the annealed oligos (guideRNA397FW: CACCGTCATCCTCCGTGATATCAGC; RV: AAACGCTGATATCACGGAGGATGAC; guideRNA64FW: CACCGTGTTAGTGGGTGCTGCCTAA; RV: AAACTTAGGCAGCACCCACTAACAC) were ligated and transformed into DH5 alpha cells. HCT116 cells were transfected with gRNA combined by pair. 24 h after, the cells were treated with 1 µg/mL puromycin and the surviving cells were diluted in 96 well plates to obtain 0.5 cells per well. Bulk cells were kept for validation. Two weeks later, cellular genomic DNA was extracted. Cells were lysed in 50 mM Tris-HCl [pH 8.0]; 100 mM EDTA [pH 8.0], 100 mM NaCl, 1% SDS and 0.1 mg of proteinase K, and incubated overnight at 55°C. 50 ng of genomic DNA were amplified with GoTaq (Promega) using primers (IDT) able to detect the deletion, (SFPQ FW: TGGGTGTATCATCCAGTTCGG; RV: GCAGAGGTCTCTGGTGTTTGAA). PCR reactions were loaded on a 1.5% agarose gel for analysis. Wild type genomic DNA and bulk were used as controls.

SFPQ overexpression

The pCMV-myc-SFPQ wild-type (WT) (Addgene #35183) was used as a template to generate the pCMV-myc-SFPQ ΔRRM1-2 by mutagenesis using the InFusion HD kit from Clontech (catalog number 639649, Mountain View, CA, with the following primers:

ΔRRM1-2 FW: CTTACACACAGCGAACTCCTCGTCCAGTCATTGTGG; ΔRRM1-2 RV: GACTGGACGAGGAGTTCGCTGTGTGTAAGTTTTTCTC.

SFPQ +/- HCT116 cells were transfected with 1 µg of either the pCMV-myc-SFPQ WT or ΔRRM1-2, or a control (pCMV-BFP) plasmid using the Lipofectamine 2000 transfection reagent (Thermo Fisher Scientific, #11668019) diluted in Opti-MEM transfection medium according to the manufacturer's instructions during 24hrs. Then, the cells were infected with SINV-GFP at MOI of 0.1 during 24h. Supernatant and proteins lysates were recovered and analysed by plaque assay and western blot, respectively.

Data availability

The mass spectrometry proteomics data have been deposited to the ProteomeXchange Consortium via the PRIDE partner repository (Perez-Riverol et al. 2019) with the dataset identifier PXD024554

Acknowledgments

The authors would like to thank all members of the Pfeffer laboratory for discussion, Amélie Weiss for technical help with GFP quantification with the INCell Analyzer 1000 Cellular Imaging System, Dr Carla Saleh for providing the SINV WT and GFP clones and Dr Diane Griffin, for providing CAPSID and nsP2 antibodies. This work was funded by the European Research Council (ERC-CoG-647455 RegulRNA) and was performed under the framework of the LABEX: ANR-10-LABX-0036_NETRNA and ANR-17-EURE-0023, which benefits from a funding from the state managed by the French National Research Agency as part of the Investments for the future program. This work has also received funding from the People Programme (Marie Curie Actions) of the European Union's Seventh Framework Program (FP7/2007-2013) under REA grant agreement n° PCOFUND-GA-2013-609102, through the PRESTIGE program coordinated by Campus France (to EG). The mass spectrometry instrumentation was funded by the University of Strasbourg, IdEx "Equipement mi-lourd" 2015.

Author contributions

SP and EG conceived the project. SP and EG designed the work and analysed the results. EG, MM, PL, AF, JC performed the experiments. EG set up the DRIMS experiments and performed the J2-IP western blots and dot blots. JC performed the bioinformatic analysis of the proteomic data, BCWM developed the MongoDB database and the Shiny application used to analyse the mass spectrometry data, EG performed the GO-enrichment and STRING

analysis. EG performed the siRNA screen. EG and MM preformed the SFPQ knockdown experiments, the western blot and qPCR analysis, EG and PL performed the plaque assays. EG and MM performed the immunofluorescence and data acquisition, MM performed the image analysis. MM generated the SFPQ +/- cell line and set up the SFPQ-RIP, PL and EG performed and analysed SFPQ KD and SINV-GFP infections in differentiated SK-N-BE(2) cells. MM generated the SFPQ mutant plasmid, MM and EG performed the rescue experiments. PH coordinated the proteomic experiments. EG and MM drafted the manuscript and designed the figures. EG and SP wrote the manuscript with input from the other authors. SP and EG coordinated the work. SP assured funding. All authors revised the final manuscript.

References

Akhrymuk I, Frolov I, Frolova EI. 2016. Both RIG-I and MDA5 detect alphavirus replication in concentration-dependent mode. *Virology* **487**: 230–241.

Akhrymuk I, Kulemzin SV, Frolova EI. 2012. Evasion of the Innate Immune Response: the Old World Alphavirus nsP2 Protein Induces Rapid Degradation of Rpb1, a Catalytic Subunit of RNA Polymerase II. *J Virol* **86**: 7180–7191.

An H, Shelkovnikova TA. 2019. Stress granules regulate paraspeckles: RNP granule continuum at work. *Cell Stress* **3**: 385–387.

An H, Tan JT, Shelkovnikova TA. 2019. Stress granules regulate stress-induced paraspeckle assembly. *J Cell Biol* **218**: 4127–4140.

Bolte S, Cordelières FP. 2006. A guided tour into subcellular colocalization analysis in light microscopy. *J Microsc* **224**: 213–232.

Bonin M, Oberstraß J, Lukacs N, Ewert K, Oesterschulze E, Kassing R, Nellen W. 2000. Determination of preferential binding sites for anti-dsRNA antibodies on double-stranded RNA by scanning force microscopy. *RNA* **6**: 563–570.

Cao P, Luo W-W, Li C, Tong Z, Zheng Z-Q, Zhou L, Xiong Y, Li S. 2019. The heterogeneous nuclear ribonucleoprotein hnRNPM inhibits RNA virus-triggered innate immunity by antagonizing RNA sensing of RIG-I-like receptors ed. S.M. Horner. *PLOS Pathog* **15**: e1007983.

Chen EY, Tan CM, Kou Y, Duan Q, Wang Z, Meirelles G, Clark NR, Ma'ayan A. 2013. Enrichr: interactive and collaborative HTML5 gene list enrichment analysis tool. *BMC Bioinformatics* **14**: 128.

Cheng W, Chen G, Jia H, He X, Jing Z. 2018. DDX5 RNA Helicases: Emerging Roles in Viral Infection. *Int J Mol Sci* **19**: 1122.

Coolidge CJ. 2000. A new double-stranded RNA-binding protein that interacts with PKR. *Nucleic Acids Res* **28**: 1407–1417.

Cristea IM, Rozjabek H, Molloy KR, Karki S, White LL, Rice CM, Rout MP, Chait BT, MacDonald MR. 2010. Host Factors Associated with the Sindbis Virus RNA-Dependent RNA Polymerase: Role for G3BP1 and G3BP2 in Virus Replication. *J Virol* **84**: 6720–6732.

Damas ND, Fossat N, Scheel TKH. 2019. Functional Interplay between RNA Viruses and Non-Coding RNA in Mammals. *Non-Coding RNA* **5**: 7.

Dhir A, Dhir S, Borowski LS, Jimenez L, Teitell M, Rötig A, Crow YJ, Rice GI, Duffy D, Tamby C, et al. 2018. Mitochondrial double-stranded RNA triggers antiviral signalling in humans. *Nature* **560**: 238–242.

Doncheva NT, Morris JH, Gorodkin J, Jensen LJ. 2019. Cytoscape StringApp: Network Analysis and Visualization of Proteomics Data. *J Proteome Res* **18**: 623–632.

Flather D, Nguyen JHC, Semler BL, Gershon PD. 2018. Exploitation of nuclear functions by human rhinovirus, a cytoplasmic RNA virus ed. A. Palmenberg. *PLOS Pathog* **14**: e1007277.

Frolova E, Gorchakov R, Garmashova N, Atasheva S, Vergara LA, Frolov I. 2006. Formation of nsP3-Specific Protein Complexes during Sindbis Virus Replication. *J Virol* **80**: 4122–4134.

Garcia-Moreno M, Järvelin AI, Castello A. 2018. Unconventional RNA-binding proteins step into the virus-host battlefront. *Wiley Interdiscip Rev RNA* **9**: e1498.

Garcia-Moreno M, Noerenberg M, Ni S, Järvelin AI, González-Almela E, Lenz CE, Bach-Pages M, Cox V, Avolio R, Davis T, et al. 2019. System-wide Profiling of RNA-Binding Proteins Uncovers Key Regulators of Virus Infection. *Mol Cell* **74**: 196-211.e11.

Gil A, Sharp PA, Jamison SF, Garcia-Blanco MA. 1991. Characterization of cDNAs encoding the polypyrimidine tract-binding protein. *Genes Dev* **5**: 1224–1236.

Girardi E, Pfeffer S, Baumert TF, Majzoub K. 2020. Roadblocks and fast tracks: How RNA binding proteins affect the viral RNA journey in the cell. *Semin Cell Dev Biol* S1084952120300914.

Greco-Stewart VS, Thibault CS-L, Pelchat M. 2006. Binding of the polypyrimidine tract-binding protein-associated splicing factor (PSF) to the hepatitis delta virus RNA. *Virology* **356**: 35–44.

Griffin D. 2007. Alphaviruses, p 1023–1067. *Fields Virol 5th Ed Lippincott Williams Wilkins Phila PA.*

Guo Z, Li Y, Ding S-W. 2019. Small RNA-based antimicrobial immunity. *Nat Rev Immunol* **19**: 31–44.

Hentze MW, Castello A, Schwarzl T, Preiss T. 2018. A brave new world of RNA-binding proteins. *Nat Rev Mol Cell Biol* **19**: 327–341.

Hur S. 2019. Double-Stranded RNA Sensors and Modulators in Innate Immunity. *Annu Rev Immunol* **37**: 349–375.

Iida K, Hagiwara M, Takeuchi A. 2020. Multilateral Bioinformatics Analyses Reveal the Function-Oriented Target Specificities and Recognition of the RNA-Binding Protein SFPQ. *iScience* **23**: 101325.

Imamura K, Imamachi N, Akizuki G, Kumakura M, Kawaguchi A, Nagata K, Kato A, Kawaguchi Y, Sato H, Yoneda M, et al. 2014. Long Noncoding RNA NEAT1-Dependent SFPQ Relocation from Promoter Region to Paraspeckle Mediates IL8 Expression upon Immune Stimuli. *Mol Cell* **53**: 393–406.

Incarbone M, Clavel M, Monsion B, Kuhn L, Scheer H, Vantard É, Poignavent V, Dunoyer P, Genschik P, Ritzenthaler C. 2021. Immunocapture of dsRNA-bound proteins provides insight into *Tobacco rattle virus* replication complexes and reveals

Arabidopsis DRB2 to be a wide-spectrum antiviral effector. *Plant Cell* **33**: 3402–3420.

Kamel W, Ruscica V, Garcia-Moreno M, Palmalux N, Iselin L, Hannan M, Järvelin A, Noerenberg M, Moore S, Merits A, et al. 2021. *Compositional analysis of Sindbis virus ribonucleoproteins reveals an extensive co-opting of key nuclear RNA-binding proteins*. Microbiology http://biorxiv.org/lookup/doi/10.1101/2021.10.06.463336 (Accessed May 16, 2022).

Kim SS-Y, Sze L, Lam K-P. 2019. The stress granule protein G3BP1 binds viral dsRNA and RIG-I to enhance interferon-β response. *J Biol Chem* **294**: 6430–6438.

Knott GJ, Bond CS, Fox AH. 2016. The DBHS proteins SFPQ, NONO and PSPC1: a multipurpose molecular scaffold. *Nucleic Acids Res* **44**: 3989–4004.

Kula A, Gharu L, Marcello A. 2013. HIV-1 pre-mRNA commitment to Rev mediated export through PSF and Matrin 3. *Virology* **435**: 329–340.

Kuleshov MV, Jones MR, Rouillard AD, Fernandez NF, Duan Q, Wang Z, Koplev S, Jenkins SL, Jagodnik KM, Lachmann A, et al. 2016. Enrichr: a comprehensive gene set enrichment analysis web server 2016 update. *Nucleic Acids Res* **44**: W90–W97.

Labeau A, Fery-Simonian L, Lefevre-Utile A, Pourcelot M, Bonnet-Madin L, Soumelis V, Lotteau V, Vidalain P-O, Amara A, Meertens L. 2022. Characterization and functional interrogation of the SARS-CoV-2 RNA interactome. *Cell Rep* **39**: 110744.

Landeras-Bueno S, Jorba N, Pérez-Cidoncha M, Ortín J. 2011. The Splicing Factor Proline-Glutamine Rich (SFPQ/PSF) Is Involved in Influenza Virus Transcription ed. A. Pekosz. *PLoS Pathog* **7**: e1002397.

LaPointe AT, Gebhart NN, Meller ME, Hardy RW, Sokoloski KJ. 2018. Identification and Characterization of Sindbis Virus RNA-Host Protein Interactions ed. M.S. Diamond. *J Virol* **92**: e02171-17, /jvi/92/7/e02171-17.atom.

Lim YW, James D, Huang J, Lee M. 2020. The Emerging Role of the RNA-Binding Protein SFPQ in Neuronal Function and Neurodegeneration. *Int J Mol Sci* **21**: 7151.

Lin J-Y, Shih S-R, Pan M, Li C, Lue C-F, Stollar V, Li M-L. 2009. hnRNP A1 Interacts with the 5′ Untranslated Regions of Enterovirus 71 and Sindbis Virus RNA and Is Required for Viral Replication. *J Virol* **83**: 6106–6114.

Liu G, Gack MU. 2020. Distinct and Orchestrated Functions of RNA Sensors in Innate Immunity. *Immunity* **53**: 26–42.

Lloyd RE. 2015. Nuclear proteins hijacked by mammalian cytoplasmic plus strand RNA viruses. *Virology* **479–480**: 457–474.

López P, Girardi E, Mounce BC, Weiss A, Chane-Woon-Ming B, Messmer M, Kaukinen P, Kopp A, Bortolamiol-Becet D, Fendri A, et al. 2020. High-Throughput Fluorescence-Based Screen Identifies the Neuronal MicroRNA miR-124 as a Positive Regulator of Alphavirus Infection ed. B.R.G. Williams. *J Virol* **94**: e02145-19, /jvi/94/9/JVI.02145-19.atom.

Montavon TC, Baldaccini M, Lefèvre M, Girardi E, Chane-Woon-Ming B, Messmer M, Hammann P, Chicher J, Pfeffer S. 2021. Human DICER helicase domain recruits PKR and modulates its antiviral activity. *PLoS Pathog* **17**: e1009549.

Nagy PD, Pogany J. 2012. The dependence of viral RNA replication on co-opted host factors. *Nat Rev Microbiol* **10**: 137–149.

Nakagawa S, Yamazaki T, Hirose T. 2018. Molecular dissection of nuclear paraspeckles: towards understanding the emerging world of the RNP milieu. *Open Biol* **8**: 180150.

Novoa RR, Calderita G, Arranz R, Fontana J, Granzow H, Risco C. 2005. Virus factories: associations of cell organelles for viral replication and morphogenesis. *Biol Cell* **97**: 147–172.

Patton JG, Mayer SA, Tempst P, Nadal-Ginard B. 1991. Characterization and molecular cloning of polypyrimidine tract-binding protein: a component of a complex necessary for pre-mRNA splicing. *Genes Dev* **5**: 1237–1251.

Pennemann FL, Mussabekova A, Urban C, Stukalov A, Andersen LL, Grass V, Lavacca TM, Holze C, Oubraham L, Benamrouche Y, et al. 2021. Cross-species analysis of viral nucleic acid interacting proteins identifies TAOKs as innate immune regulators. *Nat Commun* **12**: 7009.

Perez-Riverol Y, Csordas A, Bai J, Bernal-Llinares M, Hewapathirana S, Kundu DJ, Inuganti A, Griss J, Mayer G, Eisenacher M, et al. 2019. The PRIDE database and related tools and resources in 2019: improving support for quantification data. *Nucleic Acids Res* **47**: D442–D450.

Protter DSW, Parker R. 2016. Principles and Properties of Stress Granules. *Trends Cell Biol* **26**: 668–679.

Schlee M, Hartmann G. 2016. Discriminating self from non-self in nucleic acid sensing. *Nat Rev Immunol* **16**: 566–580.

Schonborn J, Oberstraβ J, Breyel E, Tittgen J, Schumacher J, Lukacs N. 1991. Monoclonal antibodies to double-stranded RNA as probes of RNA structure in crude nucleic acid extracts. *Nucleic Acids Res* **19**: 2993–3000.

Stetson DB, Medzhitov R. 2006. Type I Interferons in Host Defense. *Immunity* **25**: 373–381.

Varjak M, Saul S, Arike L, Lulla A, Peil L, Merits A. 2013. Magnetic Fractionation and Proteomic Dissection of Cellular Organelles Occupied by the Late Replication Complexes of Semliki Forest Virus. *J Virol* **87**: 10295–10312.

Watson SF, Bellora N, Macias S. 2019. ILF3 contributes to the establishment of the antiviral type I interferon program. *Nucleic Acids Res* gkz1060.

White E, Schlackow M, Kamieniarz-Gdula K, Proudfoot NJ, Gullerova M. 2014. Human nuclear Dicer restricts the deleterious accumulation of endogenous double-stranded RNA. *Nat Struct Mol Biol* **21**: 552–559.

Wickham L, Duchaîne T, Luo M, Nabi IR, DesGroseillers L. 1999. Mammalian Staufen Is a Double-Stranded-RNA- and Tubulin-Binding Protein Which Localizes to the Rough Endoplasmic Reticulum. *Mol Cell Biol* **19**: 2220–2230.

Wu Y, Zhao W, Liu Y, Tan X, Li X, Zou Q, Xiao Z, Xu H, Wang Y, Yang X. 2018. Function of HNRNPC in breast cancer cells by controlling the dsRNA□induced interferon response. *EMBO J* **37**. https://onlinelibrary.wiley.com/doi/abs/10.15252/embj.201899017 (Accessed November 29, 2020).

Yarosh CA, Iacona JR, Lutz CS, Lynch KW. 2015. PSF: nuclear busy-body or nuclear facilitator?: Polypyrimidine tract-binding protein-associated splicing factor. *Wiley Interdiscip Rev RNA* **6**: 351–367.

You F, Sun H, Zhou X, Sun W, Liang S, Zhai Z, Jiang Z. 2009. PCBP2 mediates degradation of the adaptor MAVS via the HECT ubiquitin ligase AIP4. *Nat Immunol* **10**: 1300–1308.

Zhang Z, Carmichael GG. 2001. The Fate of dsRNA in the Nucleus. *Cell* **106**: 465–476.

Zhou B, Wu F, Han J, Qi F, Ni T, Qian F. 2019. Exploitation of nuclear protein SFPQ by the encephalomyocarditis virus to facilitate its replication. *Biochem Biophys Res Commun* **510**: 65–71.

Figure legends

Figure 1. Identification of the dsRNA-associated proteome upon SINV infection in HCT116 cells. A) Schematic representation of SINV RNA replication and formation of dsRNA intermediates. Capped and polyadenylated viral genomic RNA is represented in black, while viral antigenomic RNA is in green. Grey arrows represent dsRNA replication. ORF1 codes for the non-structural proteins necessary for RNA replication (in orange). ORF2 codes for the structural proteins (in purple). **B**) Schematic representation of the DRIMS experimental approach. **C)** Representative dot blot revealed using the anti-dsRNA J2 antibody on RNA extracted from total lysate (INPUT), dsRNA-IP (J2)- or control-IP (IgG) in mock and SINV-infected HCT116 cells. **D)** RT-qPCR on SINV genomic (g)RNA upon dsRNA-IP (J2-IP) compared to control-IP (IgG-IP) on infected samples. Enrichment on three independent IP from three biological replicates are shown. Error bars represent mean +/- standard deviation (SD).

Figure 2. The network of dsRNA enriched proteins upon SINV infection in HCT116 cells. **A)** Volcano plot showing the global enrichment of proteins upon dsRNA-IP (J2-IP) in SINV-infected *versus* mock condition using data from three replicates. Infection conditions: 24 hours at MOI of 0.1. Red and blue dots represent proteins which are significantly enriched or depleted (adjusted p-value < 0.05, a minimum of 5 SpC in the most abundant condition, and abs(Log2FC) > 1), respectively, in the infected samples compared to the uninfected ones. Viral non-structural and structural proteins are indicated in orange and purple, respectively. Known dsRNA binding proteins are indicated in black and by a black square. Proteins present in paraspeckles are indicated in light blue and by a black hexagon. **B)** Visualization of the interaction network of proteins identified by DRIMS upon infection, generated with the Cytoscape StringApp. The confidence score of each interaction is mapped to the edge thickness and opacity. The size of the node relates to the enrichment in log2 fold change (log2FC) over the J2-IP mock control. The protein abundance in the SINV-J2 IP sample is illustrated by a colour scale and corresponds to the specific spectral count. Proteins were clustered into different functional categories using STRING enriched terms as a guideline. Proteins with dsRNA binding domain according to STRING enrichment (category: SMART domains) are highlighted in orange. **C)** Representative western blots performed on total lysate (INPUT), J2 or IgG IP in mock and SINV-GFP-infected cells using the indicated specific

antibodies. Histone 3 (H3) and HNRNPA1 were used as negative controls. * corresponds to an unspecific band.

Figure 3. SFPQ knock-down reduces SINV-GFP infection in HCT116 cells. A) Functional validation of 37 dsRNA-enriched proteins in SINV-J2 DRIMS by siRNA-based knockdown and GFP fluorescence intensity measurement of SINV-GFP infected HCT116 cells with the INCell Analyzer 1000 Cellular Imaging and Analysis System (GE Healthcare). SiRNA with a significant effect on GFP accumulation relative to siCTRL (negative control, white bar) are shown in black. SiRNA against PKR mRNA (red bar) or SINV RNA (blue bar) were used as positive controls. Data from three independent biological replicates are shown. Error bars represent mean +/- SEM of three independent experiments * $p<0.05$, ** $p < 0.01$, unpaired Student's t test. **B)**. Representative pictures of SINV-GFP infected cells in siCTRL and siSFPQ treated HCT116 cells**.** GFP expression was measured by microscopy. BF, brightfield. **C**) Representative western blot performed on mock and SINV-infected cells upon siCTRL and siSFPQ treatment. Antibodies directed against SFPQ and the viral capsid protein were used. GAPDH was used as loading control. **D)** Viral production of SINV-GFP upon siCTRL and siSFPQ transfection measured by plaque assay on three independent biological replicates. **E)** RT-qPCR on SINV genomic RNA relative to GAPDH upon siSFPQ treatment compared to siCTRL, in mock and SINV-GFP infected HCT116 cells. Data from three independent biological replicates are shown relative to siCTRL. Error bars in (D) and (E) represent mean +/- standard deviation (SD) of three independent experiments, *** $p < 0.001$, **** $p < 0.0001$, unpaired Student's t test.

Figure 4. SFPQ CRISPR/Cas9 knockout in HCT116 cells reduces SINV-GFP infection. A) Schematic representation of the CRISPR/Cas9 knockout strategy used to generate the SFPQ +/- HCT116 cells. Two gRNAs spanning the exon2/intron2 junction were used to direct Cas9 cleavage and the deletion of about 300 bp including the intron 2 5'splice site (5'ss). **B**) Agarose gel showing the PCR fragments corresponding to the WT and KO alleles respectively. Sequencing of the PCR fragment corresponding to the KO allele is shown in (A). **C-D-E)** Effect of SFPQ heterozygous knockout in HCT116 cells. **C)** Representative pictures of SINV-GFP infected cells in WT and SFPQ+/- HCT116 cells**.** GFP expression was measured by microscopy. BF, brightfield **D)** Representative western blot performed on mock and infected cells in WT and SFPQ+/- HCT116 cells. Antibodies directed against SFPQ and

the viral capsid protein were used. Tubulin was used as loading control. **E)** Viral production of SINV-GFP in WT and SFPQ+/- HCT116 cells measured by plaque assay on three independent biological replicates. Infection conditions: 24 hours at MOI of 0.1. Error bars represent mean +/- SD of three independent experiments, ** $p < 0.01$, unpaired Student's t test.

Figure 5. SFPQ sub-cellular localization in mock and SINV infected HCT116 cells. A) Confocal immunofluorescence analysis on HCT116 cells in mock and SINV WT infection conditions. Antibodies against selected factors were used (yellow signal). Antibody against dsRNA (J2) was used as a positive control of infection. DAPI was used to stain the nuclei (in blue in the merge). Magnification 20X(4X). **B**) Western blot against SFPQ upon cell fractionation on HCT116 cells in mock and SINV GFP infection conditions. Antibodies against histone 3 (H3) and Paxillin were used to control the nuclear and cytoplasmic fraction respectively. GFP was used as a control of the infection. **C**) Confocal immunofluorescence analysis on mock and SINV WT infected HCT116 cells. Antibodies against SFPQ (in purple) or dsRNA (J2 antibody, in yellow) were used. DAPI was used to stain the nuclei (in grey). Magnification 63X(3X). Red squares: 4X higher magnification. Pearson's coefficient between SFPQ and J2 0.49+/-0.1. Colocalization was quantified as Pearson's coefficient using JACoP, ImageJ plugin (Bolte and Cordelières 2006) as mean of 8 values from independent pictures +/- SD. Colocalization range from 0 to 1 (0= absence of colocalization; 1= 100% colocalization).

Figure 6. SFPQ binds to dsRNA upon infection. A) SFPQ immunoprecipitation on mock and SINV-infected HCT116 samples analysed by western blot with anti-SFPQ antibody. * corresponds to IgG L and H chains. **B)** Representative dot blot revealed using the anti-dsRNA J2 antibody on RNA extracted from total lysate (INPUT, four 10-fold dilutions), SFPQ- or IgG control-IP in mock (upper part) and SINV-infected (lower part) HCT116 cells. **C)** RT-qPCR on SFPQ-IP and IgG CTRL-IP samples by using oligos to amplify SINV genomic RNA. The fold change of SFPQ-IP over the IgG IP is shown for three biological replicates and is normalized over the INPUT (total RNA). The IgG RIP was set at 1 and represent the background signal. **D-E-F-G)** Effect of myc-SFPQ WT and ΔRRM1-2 overexpression on SINV infection. **D)** Schematic representation of myc-SFPQ wild-type and ΔRRM1-2 protein architecture. The well characterized RNA recognition motifs (RRM) 1 and

2, the NonA/paraspeckle (NOPS) and the coiled-coil domains are indicated. The less characterized GPQ-rich region, the DNA-binding domain (DBD) and the G-rich region are indicated in dashed boxes (adapted from (Knott et al. 2016))**. E)** Representative pictures of SINV-GFP in SFPQ +/- KO HCT116 cells transfected with a control, a myc-SFPQ WT or a myc-SFPQ delta RRM1-2 plasmid**.** GFP expression was measured by microscopy. BF, brightfield. **F**) Representative western blot performed on mock and SINV-infected cells upon plasmid transfection. Antibodies directed against the myc-tag and the viral capsid protein were used. Tubulin was used as loading control. **G)** Fold change of SINV-GFP viral production upon plasmid transfection measured by plaque assay on three independent biological replicates. ** $p < 0.01$ unpaired Student's t test.

Supplementary figure legends

Table S1 Details of the differential expression analysis results obtained for the enriched proteins in SINV-J2-IP versus mock-J2-IP.

Figure S1. DsRNA-associated protein profiles in mock and upon SINV infection in HCT116 cells A) Silver-stained 4-20% Tris-SDS-PAGE gel of the total lysates (INPUT) and eluates from J2 or IgG control IP in mock and SINV-infected cells used for proteomic analysis. **B)** Hierarchical clustering of the J2-IP SINV (in orange) and mock (in green) infected samples. **C-D)** Volcano plots of dsRNA-IP (J2-IP) versus IgG control-IP **(C)** in SINV-infected and **(D)** in mock-infected conditions using data from three replicates. Red and blue dots represent proteins which are significantly enriched or depleted (adjusted p-value < 0.05, a minimum of 5 SpC in the most abundant condition and abs(Log2FC) > 1), respectively, in the J2-IP samples compared to the IgG control-IP ones. Viral non-structural proteins are indicated in orange. Known dsRNA binding proteins are indicated by a black square. Proteins present in paraspeckles are indicated by a black circle and a light blue name. **E)** GO term enrichment analysis of the dsRNA-associated proteins overrepresented in SINV-J2-IP compared to mock-J2-IP using the Enrichr software. Enriched GO terms of molecular functions (green), cellular components (yellow) and biological processes (purple) are respectively sorted by p-value.

Figure S2: A) Representative pictures of SINV-GFP infected cells in siCTRL and siSFPQ treated SK-N-BE(2) cells**.** GFP expression was measured by microscopy. BF, brightfield. **B**) Representative western blot performed on non-transfected (NT) mock and infected cells and on SINV-GFP infected cells upon siCTRL and siSFPQ treatment. Antibodies directed against SFPQ and the viral capsid protein were used. Tubulin was used as loading control. **C)** Viral production of SINV-GFP upon siCTRL and siSFPQ transfection measured by plaque assay on three independent biological replicates. Infection conditions: 24 hours at MOI of 0.1. Error bars represent mean +/- SD of three independent experiments, ** $p < 0.01$, unpaired Student's t test.

Figure S3. **SFPQ binding to dsRNA is not mediated by ssRNA. A)** Representative anti-SFPQ western blot performed on total lysate (INPUT), dsRNA (J2)- or IgG control-IP in mock and SINV infected HCT116 cells with or without RNase T1 treatment. Antibodies against PKR (positive control, dsRBP) and AGO2 (negative control, ssRBP) were used. **B)** RNA analysis on agarose gel upon RNase T1 treatment on mock and SINV infected total lysate.

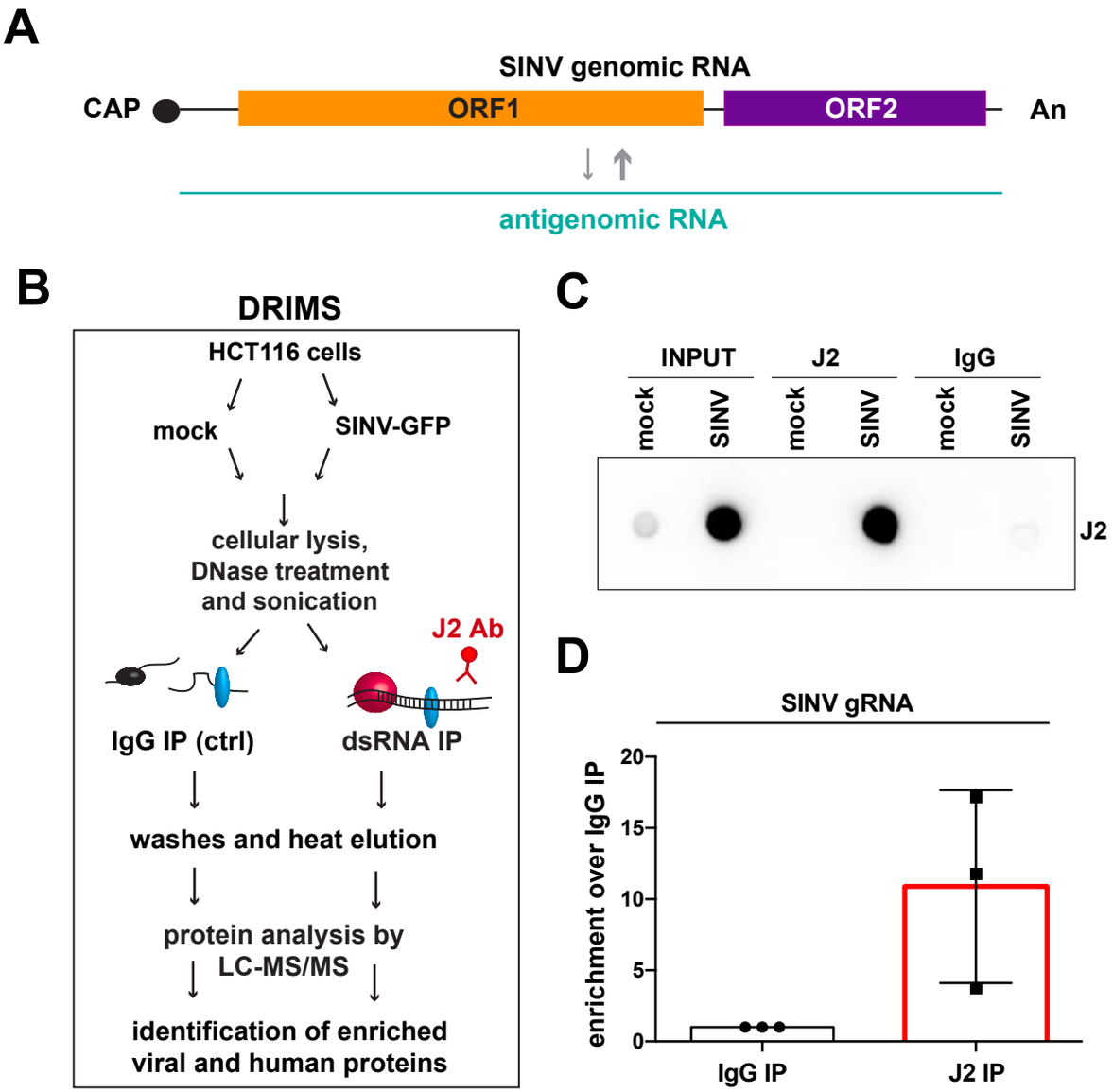
A
SINV genomic RNA
CAP
ORF1
ORF2
An
antigenomic RNA
B
DRIMS
HCT116 cells
mock
SINV-GFP
cellular lysis,
DNase treatment
and sonication
J2 Ab
IgG IP (ctrl)
dsRNA IP
washes and heat elution
protein analysis by
LC-MS/MS
identification of enriched
viral and human proteins
C
INPUT
J2
IgG
mock
SINV
mock
SINV
mock
SINV
J2
D
SINV gRNA
enrichment over IgG IP
20
15
10
5
0
IgG IP
J2 IP

Figure 1

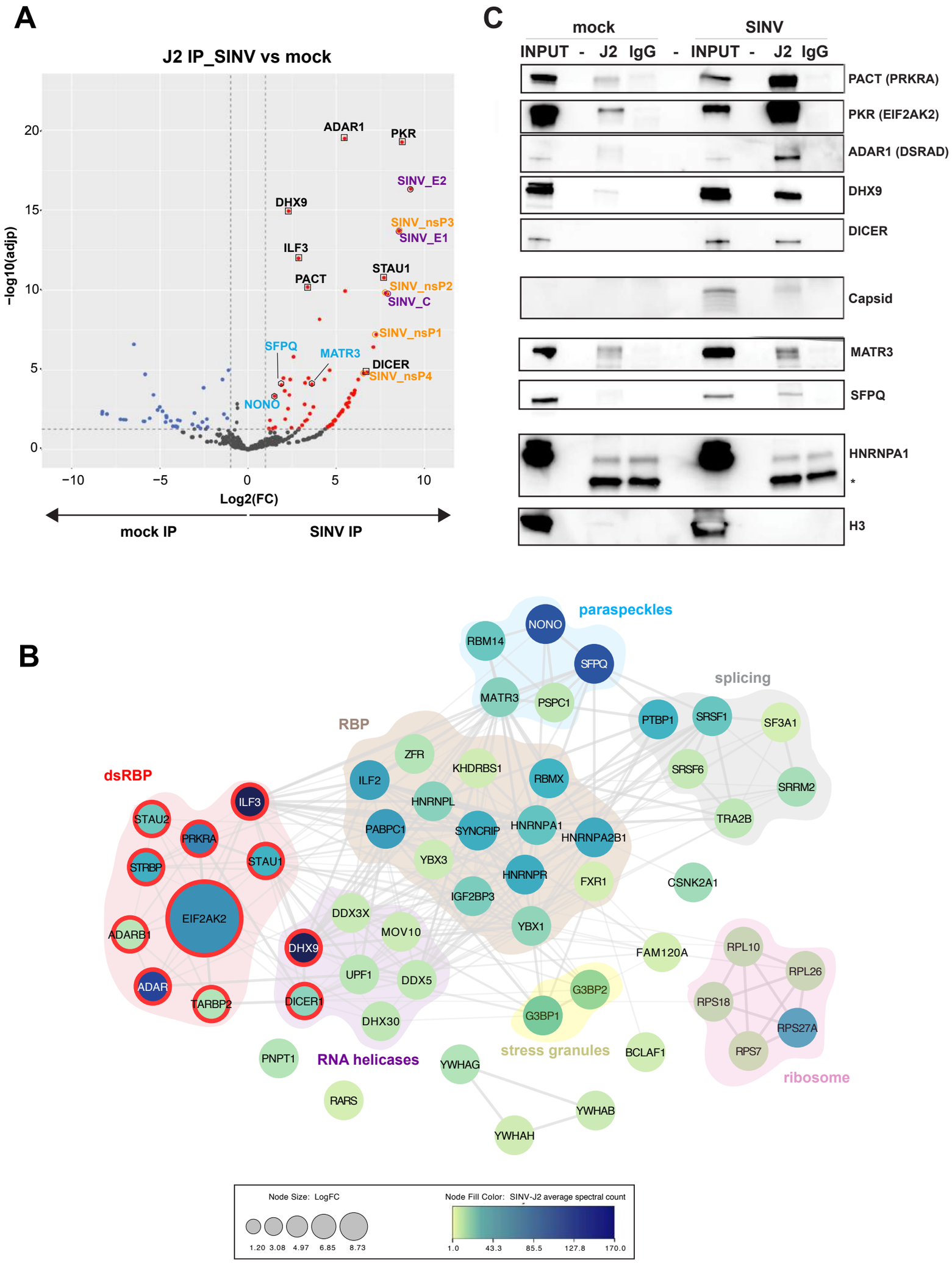
A
J2 IP_SINV vs mock
−log10(adjp)
Log2(FC)
ADAR1
PKR
SINV_E2
DHX9
SINV_nsP3
SINV_E1
ILF3
STAU1
PACT
SINV_nsP2
SINV_C
SINV_nsP1
SFPQ
MATR3
DICER
SINV_nsP4
NONO
mock IP
SINV IP
C
mock
SINV
INPUT - J2 IgG - INPUT - J2 IgG
PACT (PRKRA)
PKR (EIF2AK2)
ADAR1 (DSRAD)
DHX9
DICER
Capsid
MATR3
SFPQ
HNRNPA1
*
H3
B
paraspeckles
NONO
RBM14
SFPQ
MATR3
PSPC1
splicing
PTBP1
SRSF1
SF3A1
SRSF6
SRRM2
TRA2B
RBP
ZFR
KHDRBS1
RBMX
ILF2
HNRNPL
PABPC1
SYNCRIP
HNRNPA1
HNRNPA2B1
YBX3
HNRNPR
FXR1
CSNK2A1
IGF2BP3
YBX1
dsRBP
ILF3
STAU2
PRKRA
STAU1
STRBP
EIF2AK2
ADARB1
ADAR
TARBP2
DDX3X
MOV10
DHX9
DICER1
UPF1
DDX5
DHX30
FAM120A
RPL10
RPL26
RPS18
RPS27A
RPS7
G3BP2
G3BP1
stress granules
BCLAF1
ribosome
PNPT1
RNA helicases
YWHAG
RARS
YWHAB
YWHAH
Node Size: LogFC
1.20 3.08 4.97 6.85 8.73
Node Fill Color: SINV-J2 average spectral count
1.0 43.3 85.5 127.8 170.0

Figure 2

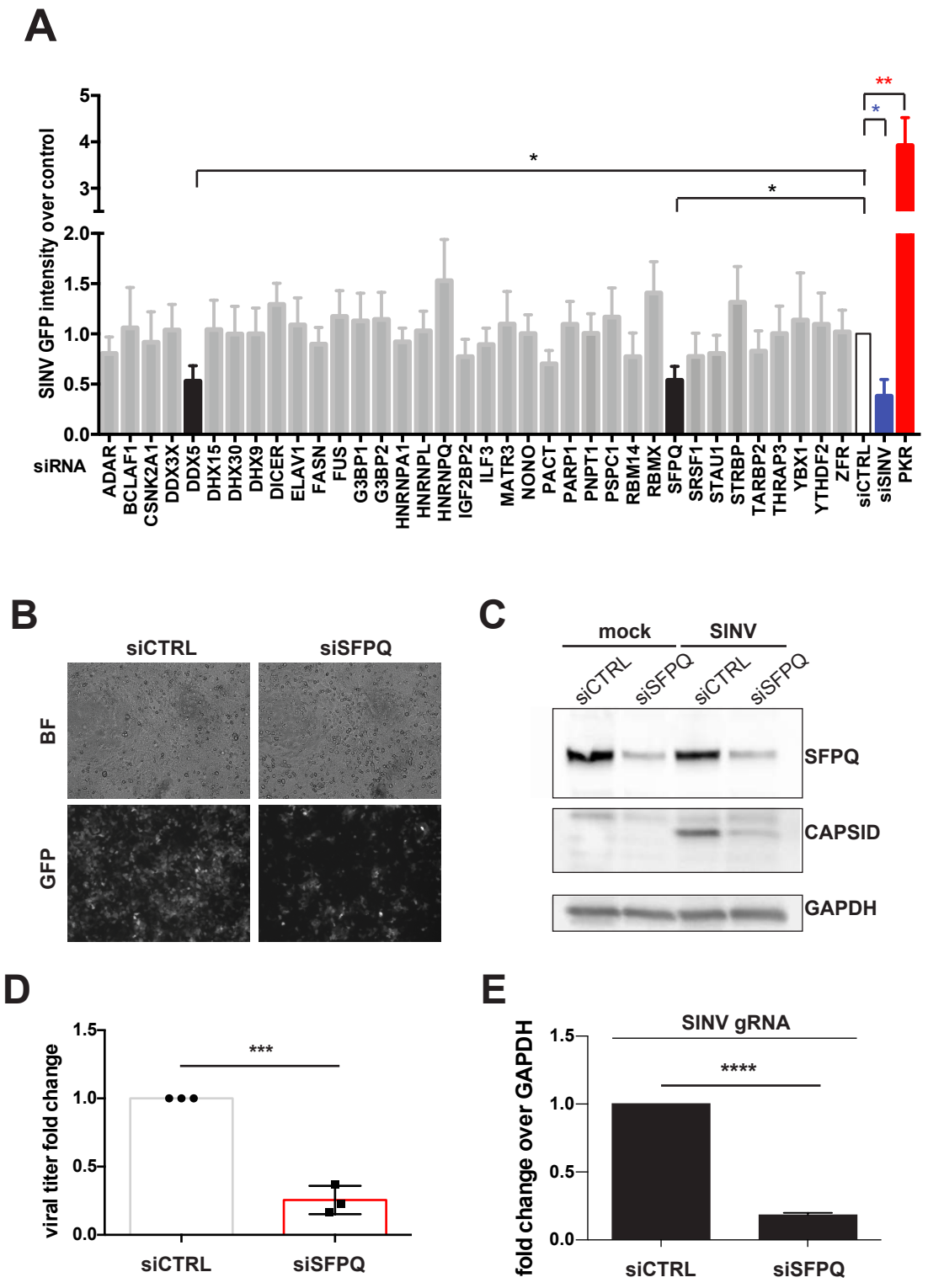
A
SINV GFP intensity over control
siRNA
ADAR
BCLAF1
CSNK2A1
DDX3X
DDX5
DHX15
DHX30
DHX9
DICER
ELAV1
FASN
FUS
G3BP1
G3BP2
HNRNPA1
HNRNPL
HNRNPQ
IGF2BP2
ILF3
MATR3
NONO
PACT
PARP1
PNPT1
PSPC1
RBM14
RBMX
SFPQ
SRSF1
STAU1
STRBP
TARBP2
THRAP3
YBX1
YTHDF2
ZFR
siCTRL
siSINV
PKR
B
siCTRL
siSFPQ
BF
GFP
C
mock
SINV
siCTRL
siSFPQ
siCTRL
siSFPQ
SFPQ
CAPSID
GAPDH
D
viral titer fold change
siCTRL
siSFPQ
E
SINV gRNA
fold change over GAPDH
siCTRL
siSFPQ

Figure 3

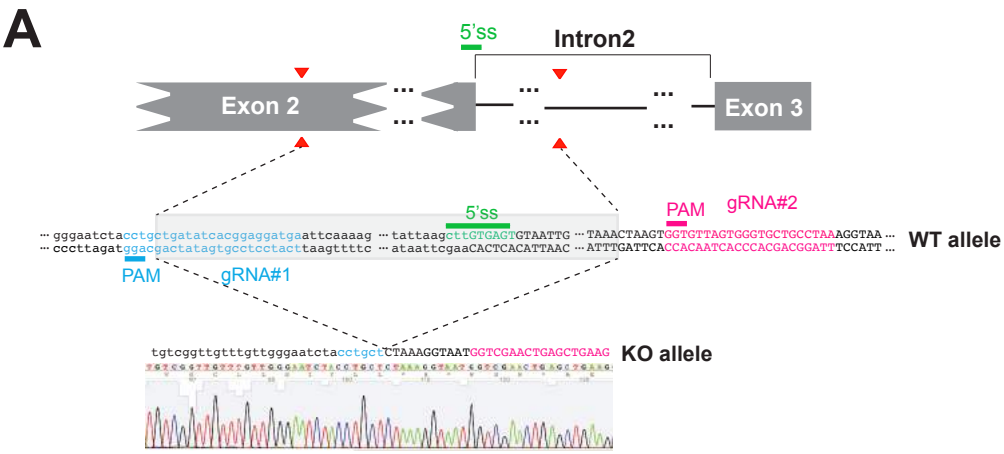
A
5'ss
Intron2
Exon 2
Exon 3
5'ss
PAM
gRNA#2
WT allele
PAM
gRNA#1
KO allele

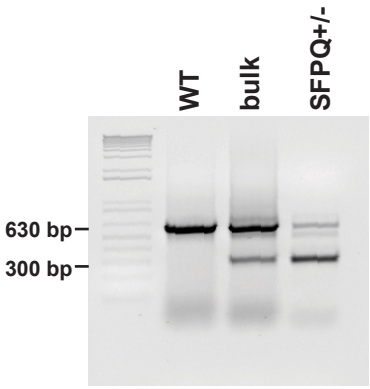
B
WT
bulk
SFPQ+/-
630 bp
300 bp

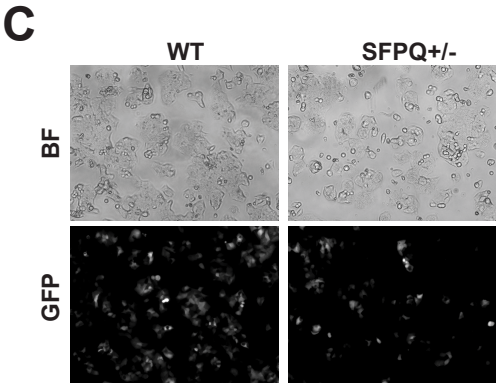
C
WT
SFPQ+/-
BF
GFP

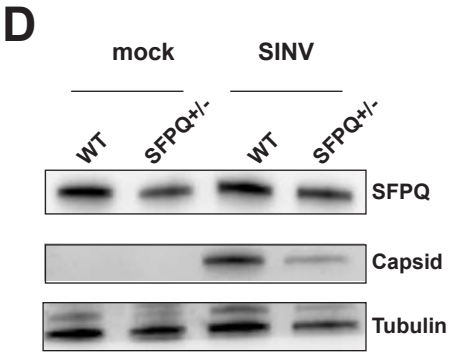
D
mock
SINV
WT
SFPQ+/-
WT
SFPQ+/-
SFPQ
Capsid
Tubulin

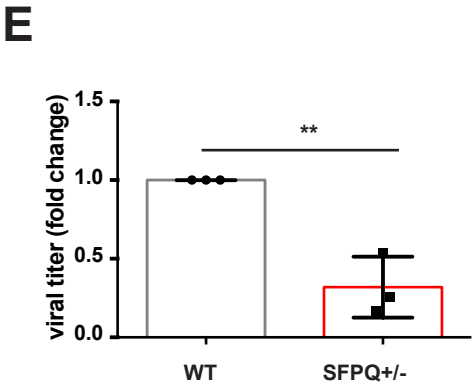
E
viral titer (fold change)
1.5
1.0
0.5
0.0
**
WT
SFPQ+/-

Figure 4

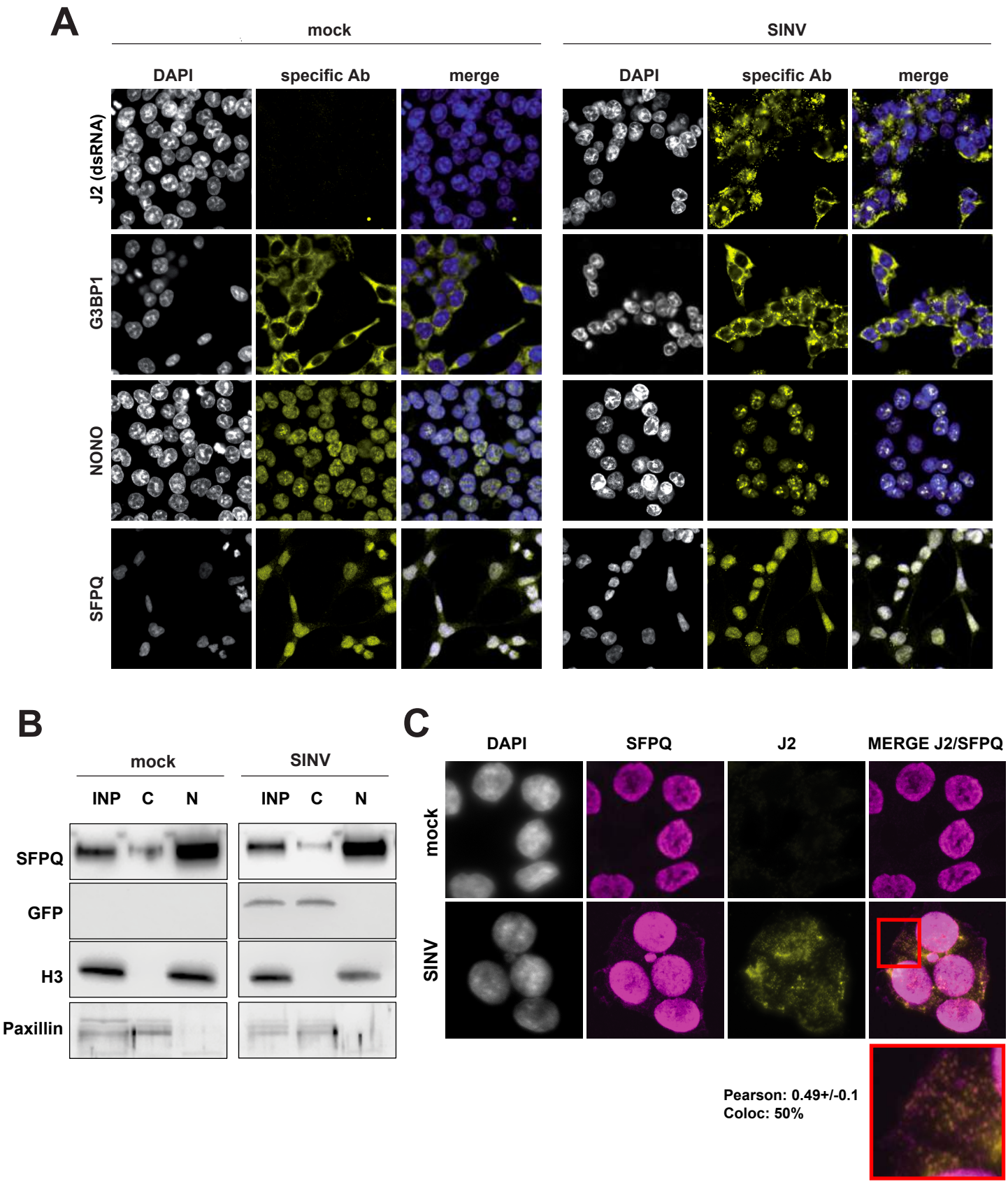
A
mock
SINV
DAPI
specific Ab
merge
DAPI
specific Ab
merge
J2 (dsRNA)
G3BP1
NONO
SFPQ
B
mock
SINV
INP
C
N
INP
C
N
SFPQ
GFP
H3
Paxillin
C
DAPI
SFPQ
J2
MERGE J2/SFPQ
mock
SINV
Pearson: 0.49+/-0.1
Coloc: 50%

Figure 5

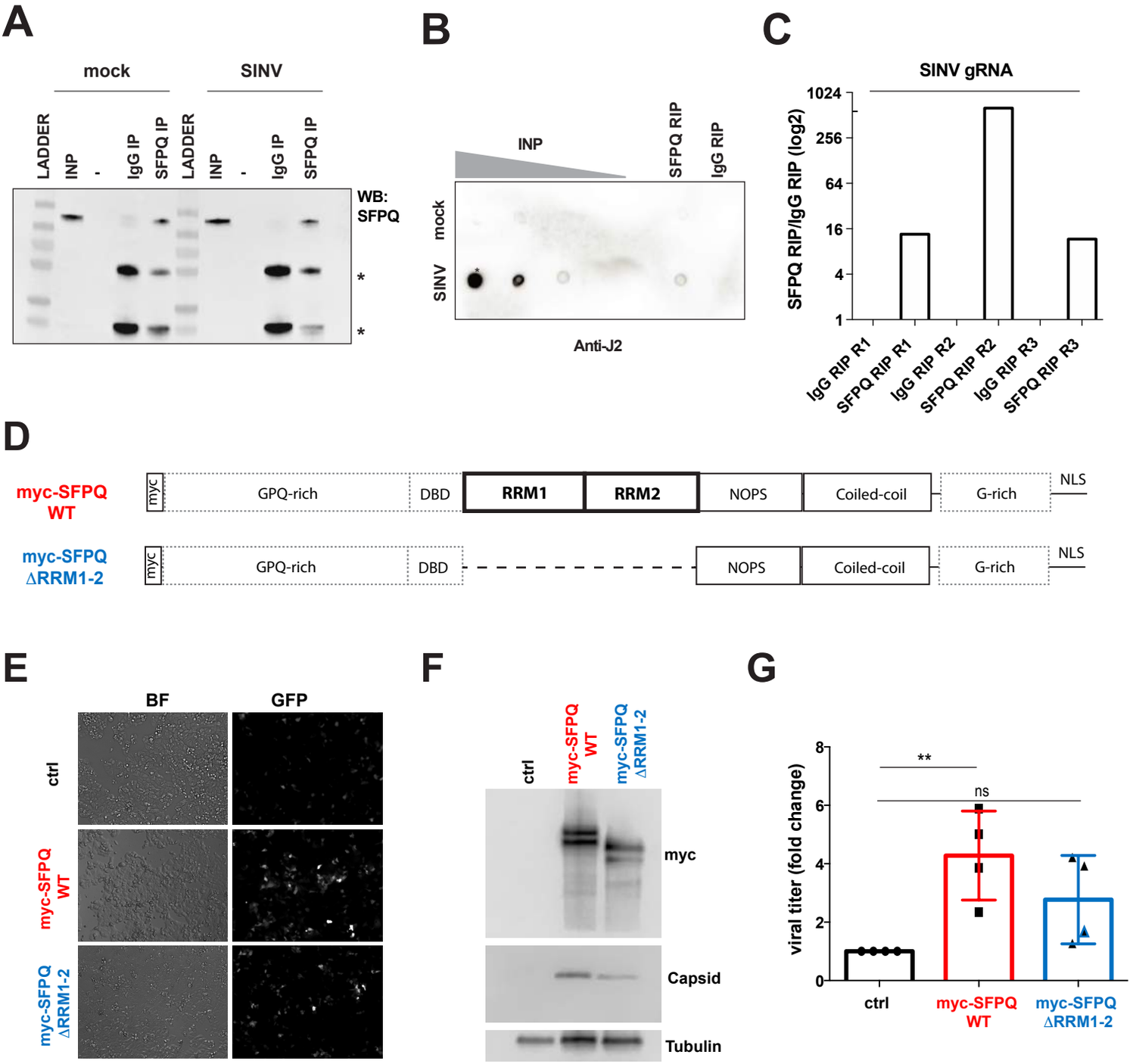
A
mock
SINV
LADDER
INP
-
IgG IP
SFPQ IP
LADDER
INP
-
IgG IP
SFPQ IP
WB:
SFPQ
*
*
B
INP
SFPQ RIP
IgG RIP
mock
SINV
Anti-J2
C
SINV gRNA
SFPQ RIP/IgG RIP (log2)
1024
256
64
16
4
1
IgG RIP R1
SFPQ RIP R1
IgG RIP R2
SFPQ RIP R2
IgG RIP R3
SFPQ RIP R3
D
myc-SFPQ WT
myc
GPQ-rich
DBD
RRM1
RRM2
NOPS
Coiled-coil
G-rich
NLS
myc-SFPQ ΔRRM1-2
myc
GPQ-rich
DBD
NOPS
Coiled-coil
G-rich
NLS
E
BF
GFP
ctrl
myc-SFPQ WT
myc-SFPQ ΔRRM1-2
F
ctrl
myc-SFPQ WT
myc-SFPQ ΔRRM1-2
myc
Capsid
Tubulin
G
viral titer (fold change)
8
6
4
2
0
**
ns
ctrl
myc-SFPQ WT
myc-SFPQ ΔRRM1-2

Figure 6